



LAWRENCE  
LIVERMORE  
NATIONAL  
LABORATORY

# Contributions of Different Cloud Types to Feedbacks and Rapid Adjustments in CMIP5

M. D. Zelinka, S. A. Klein, K. E. Taylor, T.  
Andrews, M. J. Webb, J. M. Gregory, P. M.  
Forster

August 1, 2012

Journal of Climate

## **Disclaimer**

---

This document was prepared as an account of work sponsored by an agency of the United States government. Neither the United States government nor Lawrence Livermore National Security, LLC, nor any of their employees makes any warranty, expressed or implied, or assumes any legal liability or responsibility for the accuracy, completeness, or usefulness of any information, apparatus, product, or process disclosed, or represents that its use would not infringe privately owned rights. Reference herein to any specific commercial product, process, or service by trade name, trademark, manufacturer, or otherwise does not necessarily constitute or imply its endorsement, recommendation, or favoring by the United States government or Lawrence Livermore National Security, LLC. The views and opinions of authors expressed herein do not necessarily state or reflect those of the United States government or Lawrence Livermore National Security, LLC, and shall not be used for advertising or product endorsement purposes.

# Contributions of Different Cloud Types to Feedbacks and Rapid Adjustments in CMIP5

MARK D. ZELINKA \* STEPHEN A. KLEIN, KARL E. TAYLOR,

*Program for Climate Model Diagnosis and Intercomparison, Lawrence Livermore National Laboratory, Livermore, California*

TIMOTHY ANDREWS, MARK J. WEBB

*Met Office Hadley Center, Exeter, U.K.*

JONATHAN M. GREGORY

*National Centre for Atmospheric Science, University of Reading, and Met Office Hadley Centre, Exeter, U.K.*

PIERS M. FORSTER

*University of Leeds, Leeds, U.K.*

Submitted to *Journal of Climate* 30 July 2012

## ABSTRACT

Cloud feedbacks and rapid adjustments to an abrupt quadrupling of CO<sub>2</sub> are diagnosed in five CMIP5 models using cloud radiative kernels in combination with cloud top pressure- and optical depth-partitioned cloud fractions. Upon CO<sub>2</sub> quadrupling, clouds exhibit a rapid reduction in fractional coverage, cloud top pressure, and optical depth, each contributing roughly equally to a positive global mean net cloud adjustment. Uniform rapid reductions in mid-level clouds, opposed by large increases in marine low-level cloudiness, are especially important in reducing planetary albedo in every model. As the planet warms, clouds become fewer, higher, and thicker, and global mean net cloud feedback is positive in all but one model. As in CMIP3, high cloud changes dominate the inter-model spread in LW and SW cloud feedbacks, but low cloud changes dominate that of net cloud feedback. The importance of the negative optical depth feedback relative to the amount feedback at high latitudes is even more marked than in CMIP3.

We show that the negative LW cloud adjustment inferred in previous studies is primarily caused by a 1.3 W m<sup>-2</sup> cloud masking of the CO<sub>2</sub> forcing rather than by genuine cloud changes, and that the cloud feedback is 0.3 W m<sup>-2</sup> K<sup>-1</sup> more positive when cloud masking effects are accounted for. We also show that failure to account for rapid adjustments leads to an overestimate of the positive cloud amount and altitude feedbacks and an underestimate of the negative cloud optical depth feedback, leading to a 100% overestimate of the ensemble mean net cloud feedback.

## 1. Introduction

Although 30 years have passed since the Charney report (Charney (1979)) first synthesized the state of climate science and noted the prominent role of radiative feedbacks in driving uncertainty in projections of future climate change, the current generation of climate models continues to exhibit a wide range of radiative feedbacks and climate sensitivities (Andrews et al. (2012b)). For a given increase in greenhouse gas concentration, the ensemble of models predict a range of warming magnitudes that is directly proportional to the magnitude of the radiative feedbacks that operate as the planet warms, and diversity in cloud feedbacks is consistently identified as the dominant source of this wide range (Dufresne and Bony (2008); Soden and Held (2006)). This is not surprising considering the tremendous leverage of clouds on both the longwave

(LW) and shortwave (SW) budget of the planet and the fact that they are produced from sub-grid scale parameterization schemes rather than explicitly modeled in GCMs.

The importance of clouds as feedback mechanisms has been appreciated since at least the early 1970s with the pioneering studies of Schneider (1972), Schneider and Dickinson (1974), Cess (1974), and Cess (1975), and continues to be an active area of research up to the present. In general, simulations in which the planet warms due to increased CO<sub>2</sub> exhibit an overall decrease in cloud fraction, except at high latitudes and in some tropical areas that become more favorable for convection (Wetherald and Manabe (1988); Senior and Mitchell (1993); Colman et al. (2001); Meehl et al. (2007); Zelinka et al. (2012b)). They also exhibit increased cloud top altitude as the troposphere deepens (Zelinka and Hartmann (2010); Zelinka et al. (2012b)) and an increase in high-latitude cloud optical depth due to

increases in cloud water content and phase changes (Senior and Mitchell (1993); Tsushima et al. (2006); Zelinka et al. (2012b)). These gross features are quite common to most GCM simulations. However, subtle changes to cloud properties that vary in space and time lead to significant spatio-temporal variability in the magnitudes of large and oppositely-signed cloud feedbacks, of which the global mean cloud feedback is the small residual.

Recently it has become apparent that clouds also respond directly to the greenhouse gas perturbation in such a way as to modify the radiative budget of the planet independently of their global mean surface temperature-mediated effects (Gregory and Webb (2008)). Such so-called "semi-direct" or rapid responses of clouds arise because CO<sub>2</sub> perturbations have an immediate effect on the radiative cooling rate and temperature structure of the atmosphere, even before the global mean surface temperature can respond (i.e., on a timescale of less than one month). Unlike radiative feedbacks, of which cloud feedback is one among several relevant for modifying the TOA energy balance as the planet warms, rapid adjustments to CO<sub>2</sub> are almost entirely due to cloud changes (Andrews and Forster (2008); Colman and McAvaney (2011)). It has been repeatedly shown that rapid reductions in the coverage of low clouds upon introduction of CO<sub>2</sub> play the dominant role in causing positive adjustments through the attendant reduction in planetary albedo (Andrews and Forster (2008); Colman and McAvaney (2011); Watanabe et al. (2011); Webb et al. (2012); Wyant et al. (2012)). These low cloud reductions have been attributed to decreases in relative humidity in association with CO<sub>2</sub>-induced temperature increases (Colman and McAvaney (2011)) and to shoaling of the planetary boundary layer due to suppressed surface heat fluxes (Watanabe et al. (2011)) or CO<sub>2</sub>-induced reductions in boundary layer entrainment (Wyant et al. (2012)). For a thorough review of the current state of knowledge of the cloud adjustments to CO<sub>2</sub>, see Andrews et al. (2012a).

As first pointed out in Gregory and Webb (2008), many of the radiation anomalies due to cloud changes that are commonly included as part of the cloud feedback actually occur due to rapid cloud adjustments. Webb et al. (2012) found that the contribution of variations in cloud feedback to the inter-model spread in climate sensitivity is about 4 times as large as that due to rapid cloud adjustments, though the latter is not negligible. Properly distinguishing between and quantifying the radiative implications of rapid and global mean surface temperature-mediated cloud changes is thus necessary for (1) disentangling the role of CO<sub>2</sub> from that of global mean surface temperature in causing clouds to change within a given model and (2) properly attributing inter-model spread of climate sensitivity to forcing versus feedback.

There are two main issues that cause difficulty in interpreting results from previous studies. The first is method-

ological and the second involves the choice of diagnostics. Most studies to date (excluding those listed in the previous two paragraphs) have computed cloud feedbacks by simply taking some measure of the top of atmosphere (TOA) radiative flux anomaly due to clouds between a perturbed and unperturbed climate and dividing by the global mean surface temperature change that occurred between climate states. However, rapid cloud changes that are not temperature dependent may make a substantial contribution to the TOA flux anomaly, and failing to account for them may result in an estimated feedback of the wrong magnitude and even sign (Andrews and Forster (2008)).

On the other hand, most studies – especially those evaluating an ensemble of models – that have computed the rapid cloud adjustment and cloud feedback have done so using anomalies in cloud radiative effect (*CRE*; the clear-sky all-sky upwelling radiative flux at the TOA) as their diagnostic (e.g., Andrews et al. (2012b)). As pointed out in Soden et al. (2004) and Soden et al. (2008), anomalies in *CRE* include contributions from changes in non-cloud variables in such a way as to negatively bias the derived cloud feedback. Additionally, the presence of clouds masks a portion of the radiative forcing due to CO<sub>2</sub> independent of any cloud response to it. Studies that have used more sophisticated techniques that avoid cloud masking have been performed only within a given model (e.g., Colman and McAvaney (2011); Watanabe et al. (2011); Wyant et al. (2012)), only for fixed sea surface temperature (SST) simulations with perturbed CO<sub>2</sub> (e.g., Wyant et al. (2012)), and/or only in slab ocean models (Andrews and Forster (2008)).

Thus there is a need for quantification of "true"<sup>1</sup> cloud feedbacks and rapid adjustments across an ensemble of current fully-coupled time-evolving AOGCM integrations in which cloud masking effects are avoided and surface temperature-independent cloud responses are not included in feedback estimates. It is also highly desirable to diagnose in detail the changes to cloud types and properties that are associated with feedbacks and rapid adjustments and quantify their impacts on TOA fluxes. So doing shines light on the physical mechanisms responsible for the adjustments and feedbacks and more clearly identifies the changes to cloud types and properties for which models agree and disagree.

The cloud radiative kernel technique (Zelinka et al. (2012a)) is uniquely suited to this problem. Because the radiation anomalies computed with the cloud radiative kernels are due to cloud changes alone, with no influence from non-

---

<sup>1</sup>"True" will be used hereafter to describe the TOA radiation anomalies due solely to changes in cloud properties, with no influence from non-cloud fields. We acknowledge that "true" and *CRE*-derived feedbacks and adjustments may simply be different interpretations of the influence of clouds on radiative fluxes, each with its own limitations and merits. Alternatively, one can substitute the words "unmasked" or "kernel-derived" for "true."

cloud changes, they easily provide estimates of the true cloud feedback and rapid adjustment. Furthermore, because the cloud radiative kernels quantify the sensitivity of TOA fluxes to cloud fraction perturbations for 49 different cloud types, the technique provides a quantitative partitioning of the rapid cloud adjustments and cloud feedbacks among altitude and optical depth-segregated cloud types and among changes in the overall amount, altitude, and optical depth of clouds. Finally, whereas inter-model spread in rapid adjustments and feedbacks may include some contribution from inter-model spread in radiation codes, use of the cloud radiative kernels and the International Satellite Cloud Climatology Project (ISCCP) simulator (described below) ensures a standard radiative code and definition of cloud across models, allowing for unambiguous attribution of inter-model spread to inter-model differences in cloud responses.

## 2. Data and Methodology

We make use of monthly diagnostics from abrupt4xCO<sub>2</sub>, sstClim, sstClim4xCO<sub>2</sub>, 1pctCO<sub>2</sub>, and piControl simulations of five fully-coupled ocean-atmosphere GCMs available in the Fifth Coupled Model Intercomparison Project / Second Cloud Feedback Model Intercomparison Project (CMIP5/CFMIP2) archive (Table 1). Here we adopt the CMIP5 experiment nomenclature of Taylor et al. (2012). The abrupt4xCO<sub>2</sub> runs we analyze are branched from piControl runs by instantaneously quadrupling the atmospheric CO<sub>2</sub> concentration from its preindustrial level and holding it fixed. The sstClim and sstClim4xCO<sub>2</sub> runs are atmosphere-only simulations in which climatological SSTs and sea ice from the piControl run are imposed, but with atmospheric CO<sub>2</sub> levels fixed at preindustrial and quadrupled levels, respectively. The 1pctCO<sub>2</sub> runs are forced by a compounding 1% yr<sup>-1</sup> increase in CO<sub>2</sub> from preindustrial levels, reaching quadrupled levels 140 years after branching from piControl.

Though it would be preferable to remove any residual drift that may be present in the piControl, abrupt4xCO<sub>2</sub>, and 1pctCO<sub>2</sub> runs by subtracting the trend over the entire piControl period in each variable, the limited time period over which relevant diagnostics are available precludes us from doing so. Specifically, output from the ISCCP simulator is available only for the first and last 20 years of the abrupt4xCO<sub>2</sub> run and the last 20 years of the 1pctCO<sub>2</sub> run (and the corresponding time periods in the piControl run), as called for in the CMIP5 protocol. Rather, we subtract from each of these 20-year periods the monthly mean annual cycle from the corresponding 20-year portion of the piControl run. The monthly mean climatologies in the sstClim4xCO<sub>2</sub> and sstClim runs are differenced to compute anomalies for that set of runs.

For each model (except *MPI – ESM – LR*), a twelve-

member ensemble of abrupt4xCO<sub>2</sub> simulations are analyzed, each one having branched from piControl in a different month of the year (Taylor et al. (2012)). The first ensemble member is run for the 150 year duration of the abrupt4xCO<sub>2</sub> simulation whereas the others are run only for the first 5 years following quadrupling. The monthly anomalies in each of these 5-year ensemble members are computed with respect to the monthly mean annual cycle from the corresponding 5-year portion of the piControl run. Because each ensemble member is perturbed starting in a different month, averaging across all twelve members for each month provides "monthly" resolution of the early years of the perturbed simulation while not being sensitive to the month in which the perturbation occurred.

Each model analyzed in this study implemented the ISCCP simulator (Klein and Jakob (1999); Webb et al. (2001)), which provides histograms of cloud fraction as a joint function of seven cloud top pressure (*CTP*) ranges and seven cloud optical depth ( $\tau$ ) ranges in an analogous manner to the observational ISCCP cloud products. The simulator makes use of the model's overlap assumptions to create a sub-grid distribution of clouds within each model grid box, then uses a simple radiation model to produce TOA radiances emerging from the cloudy scene. Finally, the simulator applies the same retrieval algorithm as used in ISCCP to these radiances to derive cloud properties as would be inferred from the passive ISCCP instruments. Thus the ISCCP simulator translates the modeled cloud fields into a distribution of cloud fractions in *CTP* and  $\tau$  space as ISCCP would observe for an atmosphere with the properties of the model.

The five models listed in Table 1 were chosen because they are the currently available (as of July 2012) models that performed the necessary experiments with a correctly-implemented ISCCP simulator. To verify this, we compared the model-produced total cloud fraction diagnostic (*cIt*) with the sum of the ISCCP simulator-produced cloud fraction histogram ( $C_{tot}$ ). In the models that have successfully implemented the simulator, the global mean  $C_{tot}$  minus *cIt* bias is no larger than 1.9% absolute and the RMS difference is no larger than 4.4%.

A key feature of the cloud distributions provided by the ISCCP simulator is that cloud fraction in each bin of the histogram is a "radiatively-relevant" non-overlapped cloud fraction (from a TOA perspective) that can individually impact TOA radiative fluxes. Thus, it is possible to quantify the individual contributions of changes of each cloud type to changes in the TOA LW and SW fluxes. Zelinka et al. (2012a) used a radiative transfer model (Fu and Liou (1993)) to compute sensitivities of TOA LW and SW fluxes ( $R$ ) to absolute perturbations of cloud fraction ( $C_{p\tau}$ ) of 1% in each of the 49 bins of the ISCCP histogram, which they

TABLE 1. Global climate models used in this study. The asterisk on *MPI – ESM – LR* indicates that this model provided only one abrupt4xCO2 ensemble member to the archive, whereas the other models provided twelve members. This model also did not provide output from the sstClim4xCO2 run.

Abbreviation	Modeling Center	Reference
CanESM2	Canadian Centre for Climate Modelling and Analysis	<a href="http://www.ec.gc.ca/ccmac-cccma/">http://www.ec.gc.ca/ccmac-cccma/</a> Collins et al. (2011)
HadGEM2-ES	Met Office Hadley Centre	
MIROC5	Atmosphere and Ocean Research Institute (The University of Tokyo), National Institute for Environmental Studies, and Japan Agency for Marine-Earth Science and Technology	Watanabe et al. (2010)
MPI-ESM-LR*	Max Planck Institute for Meteorology	Raddatz et al. (2007)
MRI-CGCM3	Meteorological Research Institute	Yukimoto et al. (2011)

refer to as cloud radiative kernels ( $K_{p\tau}$ ):

$$K_{p\tau} \equiv \frac{\partial R}{\partial C_{p\tau}}. \quad (1)$$

Analogous to the non-cloud kernels of Soden et al. (2008) and Shell et al. (2008), the cloud radiative kernels, when multiplied by changes in ISCCP simulator-diagnosed cloud fraction ( $\Delta C_{p\tau}$ ) between a perturbed and unperturbed climate and summed over all *CTP* and  $\tau$  categories, produce an estimate of the cloud-induced anomaly in upwelling TOA radiative fluxes ( $\Delta R_C$ ):

$$\Delta R_C = \sum_{p=1}^P \sum_{\tau=1}^T K_{p\tau} \times \Delta C_{p\tau}. \quad (2)$$

The cloud feedback is then easily computed by taking these radiative anomalies and dividing by the change in global mean surface air temperature ( $\Delta T_s$ ) between the perturbed and unperturbed climate. Zelinka et al. (2012a) showed that the cloud feedbacks computed using this technique agreed very well, both in the global mean and on a point-by-point basis with the adjusted change in cloud forcing method of Soden et al. (2008) and Shell et al. (2008), though agreement was generally better in the SW. Two of the most appealing aspects of the cloud radiative kernel method are (1) that the cloud feedback is computed directly from the changes in cloud fraction and is not influenced by changes in clear-sky fluxes and (2) that the cloud feedback at any location and month can be quantitatively attributed to changes in 49 different cloud types, giving unprecedented insight into the cloud types (e.g., high versus low and thin versus thick) as well as the changes in overall cloud properties (e.g., amount, altitude, and optical depth) that contribute to the cloud feedback.

Gregory et al. (2004) showed that the evolving change in global mean TOA radiative fluxes following an abrupt change in forcing, when plotted against  $\Delta T_s$ , closely follows a straight line, implying that the planetary energy budget

can be expressed in a simple linear form:

$$\Delta R = F + \alpha \Delta T_s, \quad (3)$$

where  $\Delta R$  is the net downwelling TOA radiative flux anomaly relative to the initial equilibrium state,  $F$  is the applied radiative forcing, and  $\alpha$  is the net climate feedback (including the Planck response and therefore negative for a stable climate).  $F$  and  $\alpha$  are both determined by least squares regression as the y-intercept and slope of the regression line, respectively.

Here we use this same diagnostic approach, but focus specifically on cloud-induced radiative flux anomalies. We plot the cloud-induced downwelling radiative flux anomaly ( $\Delta R_C$ ) computed with the cloud radiative kernels (Eq. 2) against surface temperature to derive the cloud feedback ( $\alpha_C$ ) and the instantaneous radiation perturbation due to rapid cloud adjustments ( $F_C$ ):

$$\Delta R_C = F_C + \alpha_C \Delta T_s. \quad (4)$$

Note that a positive slope ( $\alpha_C > 0$ ) implies a positive cloud feedback, and vice versa.

As will be shown below, global and annual mean values of  $\Delta R_C$  vary linearly with global mean  $\Delta T_s$ , implying  $\alpha_C$  and  $F_C$  are constants that can be estimated by ordinary least squares (OLS) linear regression of  $\Delta R_C$  on  $\Delta T_s$ . We use all twelve ensemble members' annual means in computing the regression, but each are given a weight of 1/12 during the first 5 years. The y-intercept of the regression line is an estimate of the cloud-induced radiative perturbation immediately after CO<sub>2</sub> is quadrupled and global mean  $\Delta T_s$  is still 0, which we will refer to as the rapid cloud adjustment ( $F_C$ ). The slope of the OLS regression line passing through the data points represents the change in cloud-induced radiative fluxes per increase in global mean surface temperature, the cloud feedback ( $\alpha_C$ ). Unlike the values of cloud feedback derived by plotting cloud radiative effect anomalies against surface temperature anomalies (Gregory and Webb (2008); Andrews et al. (2012b)),  $\alpha_C$

contains only the cloud-induced radiative flux anomalies with no contribution from clear-sky flux anomalies. Uncertainties in OLS regression slopes are estimated as the  $2\sigma$  range of possible regression slopes computed from 1000 bootstrapped samples with replacement.

### 3. Global Mean Rapid Cloud Adjustments and Cloud Feedbacks

In Figures 1 and 2, we show Gregory plots for cloud-related anomalies in TOA LW and SW radiative fluxes, respectively, for the five models studied. The left column contains (black) cloud-induced TOA radiative flux anomalies derived using cloud radiative kernels and (gray)  $CRE$  anomalies plotted against global mean  $\Delta T_s$  anomalies. In the right column is the breakdown of the kernel-derived cloud-induced radiation anomalies into amount, altitude, and optical depth components (discussed below). In addition, we show in red crosses the anomalies from the sstClim4xCO2 experiments, which give alternative estimates of the response of clouds to a CO<sub>2</sub> quadrupling while attempting to keep the surface from warming. Note, however, that the land surface warms, which is reflected in a global mean warming of roughly 0.5 K. We also overlay with diamonds the anomalies from the last 5 years of the 1pctCO2 runs (i.e., the five years closest to when CO<sub>2</sub> concentrations are quadrupled from pre-industrial). Tables 2 and 3 contain global mean values of LW, SW, and net rapid cloud adjustments and cloud feedbacks, respectively, for the five models analyzed.

Global mean values of  $\Delta LW_{CRE}$  and  $\Delta LW_C$  behave remarkably linearly when plotted against the  $\Delta T_s$  anomalies, and rarely deviate from the OLS regression lines. In all but one model ( $MRI - CGCM3$ ) the true LW cloud feedback is positive, though in both the  $MRI - CGCM3$  and  $MIROC5$  models, it is statistically indistinguishable from zero. Even among this relatively small ensemble of five models, the LW cloud feedback spans a considerable range, from just under 0 to  $0.8 \text{ W m}^{-2} \text{ K}^{-1}$ . The true LW cloud adjustment (y-intercept) is negative in all but the  $HadGEM2 - ES$  model, and is indistinguishable from zero in all but the  $HadGEM2 - ES$  and  $MRI - CGCM3$  models, implying that rapid cloud adjustments to quadrupled CO<sub>2</sub> have small relevance – in the global mean – for the LW budget of the planet. (Note that in the  $HadGEM2 - ES$  model, the early anomalies clearly deviate from the regression line, so even this model likely has a small negative LW cloud adjustment.) These small and generally negative values of LW cloud adjustment are consistent with those listed in Table 1 of Andrews and Forster (2008).

In contrast, the  $\Delta LW_{CRE}$ -derived feedback (plotted in gray) is considerably less positive or more negative than the true LW cloud feedback, and the rapid LW cloud adjustment is systematically large and negative, between -1.2

and  $-2.0 \text{ W m}^{-2}$ . The former is a consequence of non-cloud-induced radiative flux anomalies that are included in  $LW_{CRE}$  anomalies, primarily increases in water vapor that act to decrease clear-sky upwelling LW fluxes (Soden et al. (2004)). The latter is a consequence of cloud masking of the direct radiative forcing by CO<sub>2</sub>. Both of these processes will be discussed in greater detail below.

$\Delta SW_{CRE}$  and  $\Delta SW_C$  also behave quite linearly when plotted against the  $\Delta T_s$  anomalies, though compared with the LW, larger deviations from the OLS regression lines are apparent in the first few years after quadrupling, especially in the  $HadGEM2 - ES$  and  $MRI - CGCM3$  models (Figure 2). The SW cloud feedbacks vary considerably among the models, though unlike the LW cloud feedbacks, the signs are unconstrained, ranging from  $-0.3$  to  $0.3 \text{ W m}^{-2} \text{ K}^{-1}$ . In contrast to the consistently small LW cloud adjustments, the SW cloud adjustments vary from  $-0.6$  to  $2.1 \text{ W m}^{-2}$  and are always distinguishable from zero. The two models for which it is negative ( $HadGEM2 - ES$  and  $MRI - CGCM3$ ) exhibit obvious deviations from the regression line in the first few years of the integration, and their early anomalies are positive<sup>2</sup>. Clearly rapid cloud adjustments are much more relevant to the global mean SW budget than to the LW budget and – considering the early abrupt4xCO2 anomalies and the sstClim4xCO2 anomalies rather than the regression intercepts – tend to enhance the radiative forcing due to CO<sub>2</sub>, in accord with previous studies (Andrews and Forster (2008); Colman and McAvaney (2011); Watanabe et al. (2011); Webb et al. (2012); Wyant et al. (2012)).

$\Delta SW_{CRE}$ - and  $\Delta SW_C$ -derived rapid cloud adjustments (either from the regression intercept or from the sstClim4xCO2 runs) are consistently closer in the SW than in the LW, implying that cloud masking of the forcing is smaller in the SW, as expected. The true SW cloud feedback is consistently larger (more positive or less negative) than the  $\Delta SW_{CRE}$  "feedback" indicating that clouds mask the non-cloud SW feedbacks, primarily surface albedo feedback. This is an especially large effect in the  $MIROC5$  and  $MPI - ESM - LR$  models.

Note that in Figures 1 and 2,  $\Delta CRE$  and  $\Delta R_C$  from the 1pctCO2 runs (diamonds) lie along the regression line, and anomalies in the sstClim4xCO2 runs (red crosses) do indeed correspond closely with the early anomalies computed in the freely-evolving quadrupled CO<sub>2</sub> runs. This highlights the robustness of these anomalies for a given increase in CO<sub>2</sub> and surface temperature. That the 1pctCO2 anomalies lie along the regression line at the time in the 1pctCO2 run where the CO<sub>2</sub> is close to 4 times its preindustrial value suggests that the cloud adjustments due solely to CO<sub>2</sub> depend only on the prevailing CO<sub>2</sub> concentration, and

<sup>2</sup>For further discussion of the deviations from linearity in the early stages of the abrupt4xCO2 simulation, please refer to Section 4 of Andrews et al. (2012b).

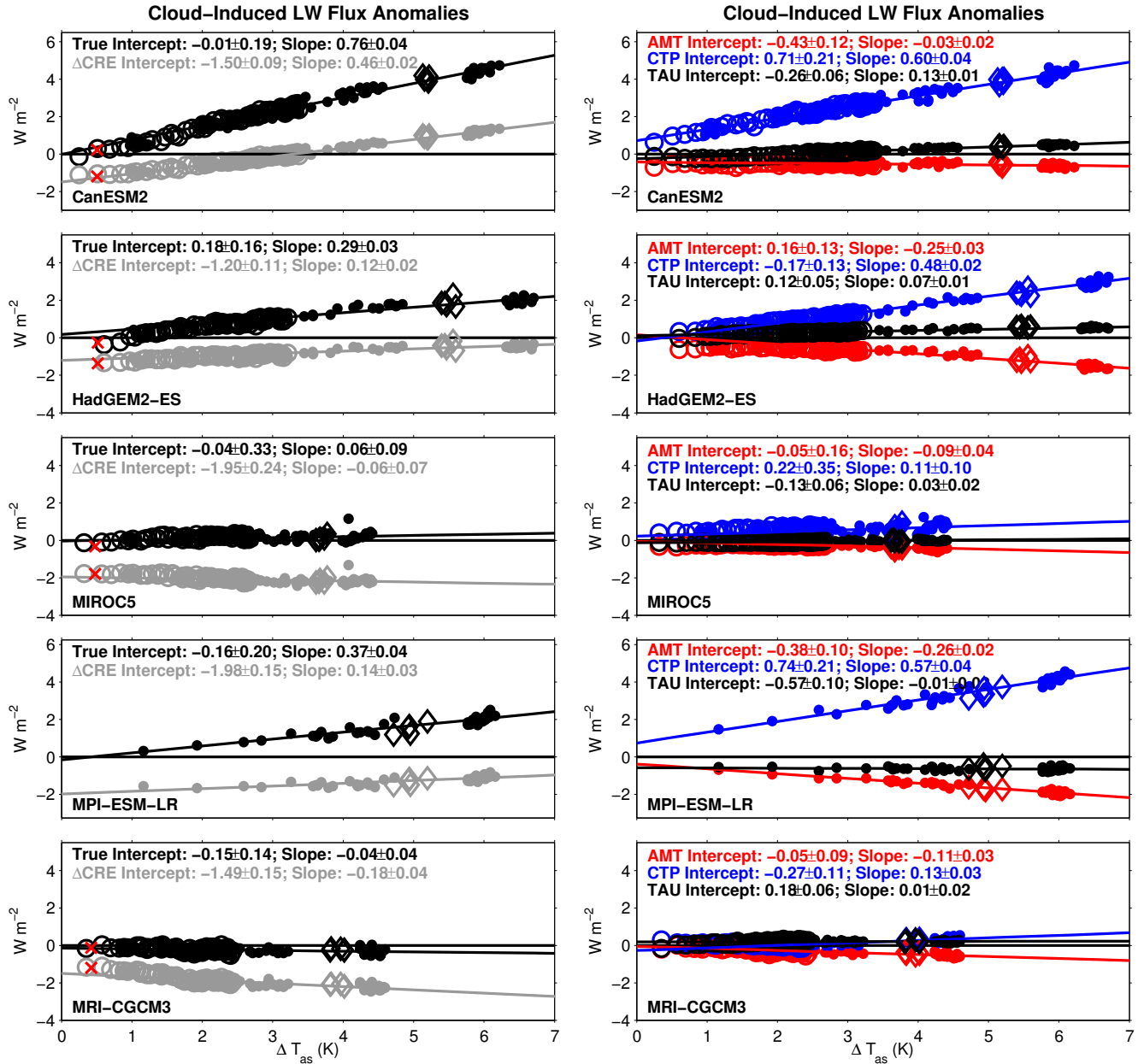


FIG. 1. (left column) Global mean anomalies in (black) cloud-induced TOA LW radiative fluxes derived using cloud radiative kernels and (gray)  $LWCRE$  plotted against anomalies in global mean  $\Delta T_s$ . Filled circles represent annual anomalies computed using the first ensemble member of the abrupt4xCO2 run. Unfilled circles represent the annually-averaged monthly resolved anomalies computed using the 12-member ensembles available for the first 5 years of the abrupt4xCO2 run. Red crosses represent the anomalies derived from the sstClim4xCO2 runs and diamonds represent the anomalies derived from the final 5 years of the 1pctCO2 runs. Lines represent the ordinary least squares regression of the abrupt4xCO2 anomalies on global mean  $\Delta T_s$ , and the y-intercept and slope of these lines are displayed in each panel, along with their 2- $\sigma$  uncertainties. (right column) As for the left column, but showing cloud-induced LW TOA fluxes partitioned into contributions from changes in cloud amount, altitude, and optical depth following Zelinka et al. (2012b).

not its history. This implies that the portion of the cloud-induced radiation anomalies due to rapid adjustments to

CO<sub>2</sub> in the 1pctCO2 runs may plausibly be explained by those seen in the abrupt4xCO2 experiments. Thus, infor-

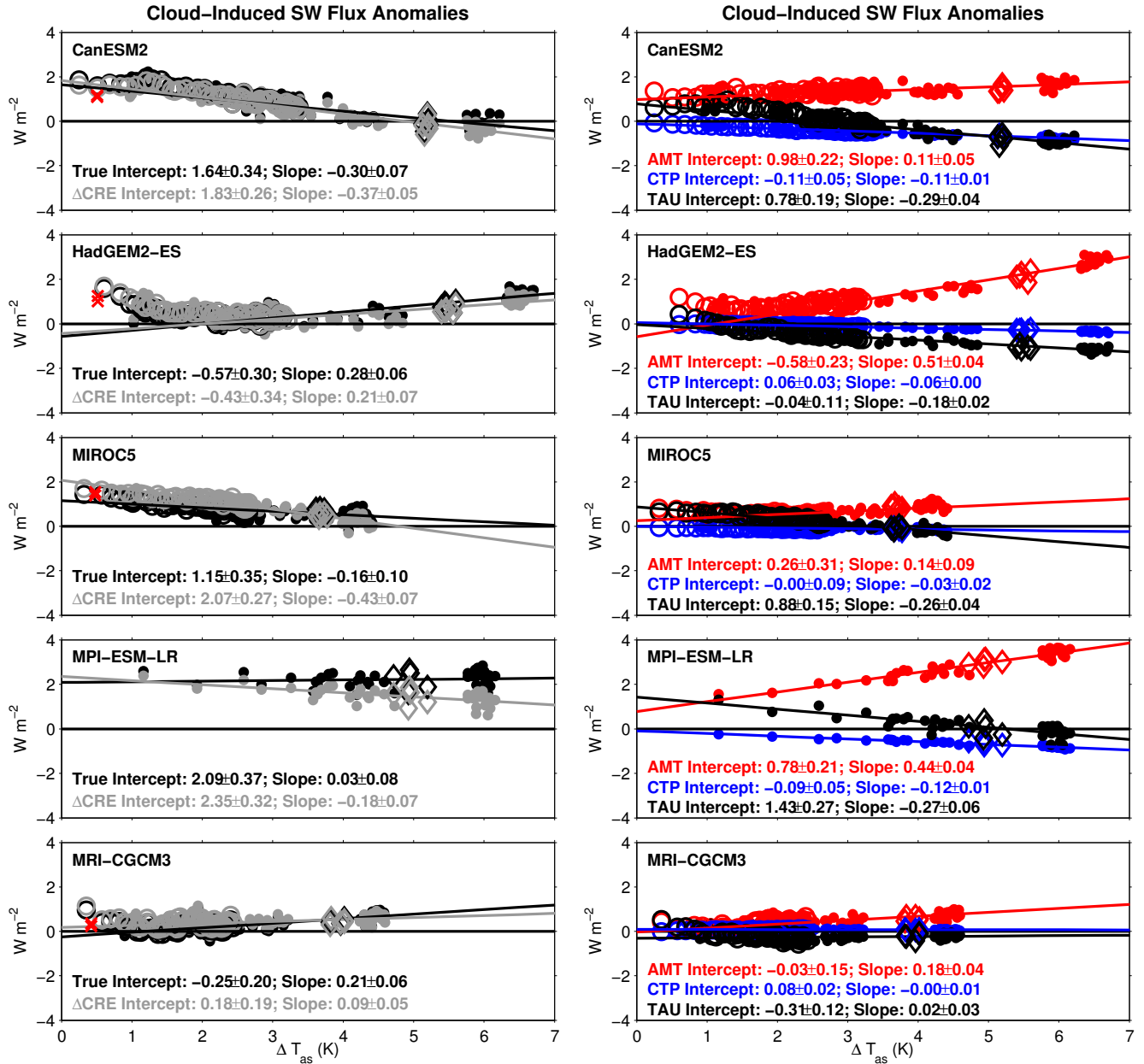


FIG. 2. Same as in Figure 1, but for SW fluxes.

mation derived from highly idealized step-function forcing experiments are relevant to more realistic transient scenarios (e.g. Good et al. (2011); Good et al. (2012)).

#### 4. Spatial Patterns of Rapid Cloud Adjustments and Cloud Feedbacks

What is the horizontal and vertical structure of the rapid cloud adjustments and cloud feedbacks? To answer this, we compute the regression of *local* cloud anomalies

onto *global mean* surface temperature anomalies. As with the global mean anomalies plotted above, the local slope represents the local cloud response per unit change in global mean surface temperature ( $\% K^{-1}$ ) which, when multiplied by the cloud radiative kernel ( $W m^{-2} \%^{-1}$ ), gives the local contribution to the cloud feedback ( $W m^{-2} K^{-1}$ ). The local cloud adjustment could be assessed by computing the average over the early part of the abrupt4xCO<sub>2</sub> run, but this may be strongly dependent on the state of ENSO in the piControl run at the time of quadrupling. It can also be

TABLE 2. Global mean LW, SW, and net rapid cloud adjustments. The intercept uncertainty for an individual model is the 95% confidence interval on the regression slope and intercept. The uncertainty in individual models’ sstClim4xCO2 estimates is the standard deviation of the 30 annual means (50 in the case of CanESM2). The uncertainty in the mean is the standard deviation across model means.

Model	Regression Line Intercept			sstClim4xCO2 Estimate		
	LW	SW	Net	LW	SW	Net
CanESM2	$-0.01 \pm 0.20$	$1.64 \pm 0.33$	$1.63 \pm 0.30$	$0.22 \pm 0.09$	$1.09 \pm 0.14$	$1.31 \pm 0.15$
HadGEM2-ES	$0.18 \pm 0.18$	$-0.57 \pm 0.28$	$-0.39 \pm 0.22$	$-0.26 \pm 0.07$	$1.01 \pm 0.13$	$0.75 \pm 0.12$
MIROC5	$-0.04 \pm 0.31$	$1.15 \pm 0.36$	$1.11 \pm 0.26$	$-0.32 \pm 0.08$	$1.54 \pm 0.15$	$1.22 \pm 0.11$
MPI-ESM-LR	$-0.16 \pm 0.20$	$2.09 \pm 0.38$	$1.93 \pm 0.31$	N/A	N/A	N/A
MRI-CGCM3	$-0.15 \pm 0.14$	$-0.25 \pm 0.20$	$-0.40 \pm 0.18$	$-0.13 \pm 0.09$	$0.24 \pm 0.11$	$0.11 \pm 0.11$
Mean	$-0.04 \pm 0.14$	$0.81 \pm 1.17$	$0.78 \pm 1.11$	$-0.12 \pm 0.24$	$0.97 \pm 0.54$	$0.85 \pm 0.55$

TABLE 3. Global mean LW, SW, and net cloud feedbacks. The uncertainty for an individual model is the 95% confidence interval on the regression slope and intercept, and the uncertainty in the mean is the standard deviation across model means.

Model	LW	SW	Net
CanESM2	$0.76 \pm 0.04$	$-0.30 \pm 0.07$	$0.46 \pm 0.06$
HadGEM2-ES	$0.29 \pm 0.03$	$0.28 \pm 0.06$	$0.57 \pm 0.04$
MIROC5	$0.06 \pm 0.09$	$-0.16 \pm 0.10$	$-0.10 \pm 0.07$
MPI-ESM-LR	$0.37 \pm 0.04$	$0.03 \pm 0.08$	$0.39 \pm 0.07$
MRI-CGCM3	$-0.04 \pm 0.04$	$0.21 \pm 0.06$	$0.17 \pm 0.05$
Mean	$0.29 \pm 0.31$	$0.00 \pm 0.24$	$0.29 \pm 0.26$

calculated as the local y-intercept from the abrupt4xCO2 run, but uncertainties in the regression slope and intercept (present even for the global means shown in Figures 1 and 2) become even larger at local scales, limiting the information content of the patterns derived in this manner. Also, using the regression slope intercept assumes that the cloud anomalies at each point followed a simple linear path from the beginning to the end of the integration, with no deviations from linearity. That this clearly does not hold in the global mean (especially for *HadGEM2 – ES*) makes it even less likely to hold at the local scale.

Alternatively, one can calculate cloud anomalies from the sstClim4xCO2 run, in which the climatological annual cycle of SST is imposed but with CO2 held at quadrupled levels. Averaging over the 30-year sstClim4xCO2 run reduces the sensitivity to the initial state of the climate and provides a more robust and stable measure of the rapid cloud adjustment to CO2. It also does not rely on the assumption that the response evolves linearly with global mean temperature. That the sstClim4xCO2 global mean anomalies (red crosses in Figures 1 and 2) tend to lie much closer to the abrupt4xCO2 anomalies in the early stages of the abrupt4xCO2 integration where they deviate most significantly from the regression line further supports their

use as a more robust measure of the true cloud adjustment than the intercept. For these reasons we have chosen to present the sstClim4xCO2 anomalies, though most features discussed below are similar regardless of the chosen measure of rapid cloud adjustment.

The ensemble mean rapid cloud adjustments partitioned into the 9 major ISCCP categories (Rossow and Schiffer (1999)) are shown in Figure 3. For all figures hereafter, shades of blue will be used to indicate positive cloud amount, *CTP*, or  $\tau$  anomalies, which tend to have a net cooling effect on the planet. The contributions of high, mid-level, and low clouds to the LW, SW, and net cloud feedbacks and rapid adjustments are shown in Table 4. One must keep in mind that changes in low clouds diagnosed by the ISCCP simulator may result from obscuration changes (e.g., an apparent decrease in low cloud fraction that is due to an increase in high cloud fraction that obscures more low clouds).

Although one might infer from Figure 1 that the consistently small global mean LW rapid cloud adjustment is evidence that there is a negligible rapid high cloud response to CO2, it is clear from Figure 3 that this is not true. High clouds of all optical thickness categories decrease significantly in the southern Indian Ocean, the Eastern Pa-

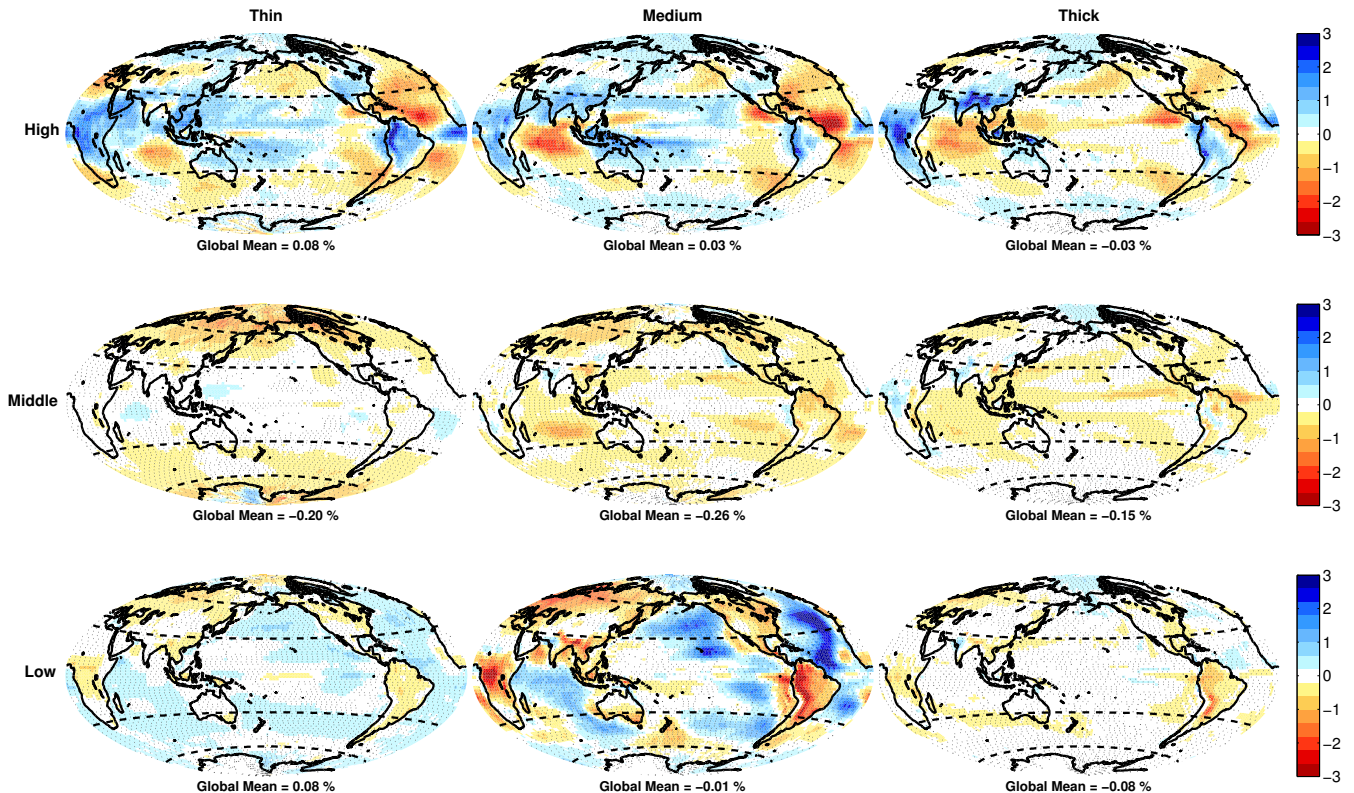


FIG. 3. Ensemble mean rapid cloud adjustments diagnosed as the 30-year average cloud anomaly from the sstClim4xCO<sub>2</sub> run partitioned into nine standard ISCCP categories. Stippling indicates locations where at least 3 out of 4 models agree on the sign of the field plotted.

cific, and throughout the Atlantic Ocean, while increasing substantially over tropical and subtropical land areas and over the Maritime Continent. In the global mean, thin and medium-thickness high clouds increase at the expense of high thick clouds, so the total high cloud increase is very small (0.08%). Low clouds of all optical thickness categories decrease substantially over land, while thin and medium-thickness low clouds increase substantially over the ocean. In the global mean, medium-thickness low cloud changes are negligible, while the decrease of thick low cloud exactly cancels the increase in thin low cloud, leading to a small positive net adjustment from low clouds (Table 4).

Medium thickness low clouds exhibit the most dramatic regional anomalies, though their global mean change is nearly zero due to large increases over ocean and decreases over land. Increases are most prominent over the eastern ocean basins where marine stratocumulus clouds are prevalent. Consistent with these large increases in low cloud, Webb et al. (2012) showed that both lower tropospheric stability (Klein and Hartmann (1993)) and estimated inversion strength (EIS; Wood and Bretherton (2006)) increase substantially upon CO<sub>2</sub> doubling in slab ocean models, and

that EIS responses are strongly negatively correlated with cloud radiative responses across models (i.e., models with greater stability increases have greater low cloud increases that impart a greater negative net radiative response), especially in the most stable regimes. Abrupt decreases in low level cloudiness are, however, apparent very near the coasts of California, Peru, Namibia, and Australia. These low cloud reductions may be caused by advection of warm and/or dry air by the easterly trade winds flowing off the adjacent warmer and drier continent (c.f. Figure 4 of Andrews et al. (2012a))

The largest global mean rapid adjustments occur for mid-level clouds, which exhibit a large global mean decrease of 0.61%, and show systematic decreases in all thickness categories in almost every location. In the ensemble mean, the contribution of rapid mid-level cloud reductions to the SW anomaly is five times larger than those of both high and low clouds (Table 4). Mid-level cloud reductions enhance the downwelling TOA net radiation by nearly twice as much high cloud anomalies, which themselves enhance the downwelling net radiation by twice as much as low cloud reductions (Table 4). This is in stark

TABLE 4. Global mean LW, SW, and net rapid cloud adjustments and cloud feedbacks separated into contributions from high ( $CTP \leq 440$  hPa), mid-level ( $440 < CTP \leq 680$  hPa), low ( $CTP > 680$  hPa), thin ( $\tau \leq 3.6$ ), medium-thickness ( $3.6 < \tau \leq 23$  hPa), and thick ( $\tau > 23$  hPa) cloud types, and their sum. Note the  $CTP$  and the  $\tau$  segregated cloud feedbacks individually sum to the total. The uncertainty is the standard deviation across model means.

Level	CloudAdjustment ( $W m^{-2}$ )			Cloud Feedback ( $W m^{-2} K^{-1}$ )		
	LW	SW	Net	LW	SW	Net
High	$0.12 \pm 0.23$	$0.14 \pm 0.17$	$0.26 \pm 0.10$	$0.32 \pm 0.38$	$-0.21 \pm 0.39$	$0.11 \pm 0.08$
Mid	$-0.24 \pm 0.07$	$0.70 \pm 0.32$	$0.46 \pm 0.25$	$-0.03 \pm 0.07$	$-0.01 \pm 0.18$	$-0.03 \pm 0.12$
Low	$-0.01 \pm 0.05$	$0.13 \pm 0.50$	$0.13 \pm 0.45$	$0.00 \pm 0.05$	$0.21 \pm 0.23$	$0.21 \pm 0.19$
Thin	$0.03 \pm 0.14$	$0.01 \pm 0.07$	$0.04 \pm 0.10$	$0.00 \pm 0.04$	$0.06 \pm 0.04$	$0.05 \pm 0.05$
Medium	$-0.05 \pm 0.09$	$0.35 \pm 0.29$	$0.30 \pm 0.25$	$0.07 \pm 0.18$	$0.28 \pm 0.22$	$0.35 \pm 0.18$
Thick	$-0.11 \pm 0.04$	$0.61 \pm 0.32$	$0.51 \pm 0.30$	$0.23 \pm 0.16$	$-0.34 \pm 0.28$	$-0.11 \pm 0.17$
Total	$-0.12 \pm 0.24$	$0.97 \pm 0.54$	$0.85 \pm 0.55$	$0.29 \pm 0.31$	$0.00 \pm 0.24$	$0.29 \pm 0.26$

contrast to the results of previous studies cited in the Introduction that identified low clouds as the primary cloud type causing large radiative adjustments, and demands some explanation.

One possible reason that we are finding large rapid responses of mid-level rather than low-level clouds as in previous studies is due to our use of the ISCCP simulator: In determining  $CTP$  for clouds under atmospheric temperature inversions, ISCCP often erroneously assigns  $CTP$  to a level far higher (100-300 hPa) in the atmosphere than it should be Garay et al. (2008), a feature which the ISCCP simulator purposely mimics. Thus it is possible that a reduction in cloud fraction near the tops of marine stratiform clouds is actually responsible for a portion of the large positive SW adjustment that we are attributing to reductions in mid-level clouds upon  $CO_2$  quadrupling. This is partially supported by the patterns of mid-level cloud anomalies, which have the largest reductions in the predominantly low cloud-dominated regions over the subtropical oceans (Figure 3). However, the fact that mid-level cloud reductions are not confined to these regions suggests that many of the reductions are real. Another possibility is that the occurrence of high thin clouds overlying low clouds – which the simulator purposely interprets as mid-level cloud – decreases upon  $CO_2$  quadrupling.

Over land, the rapid cloud adjustment is characterized by a decrease in low clouds and an increase in high clouds. This can be seen more clearly in the left column of Figure 5, which shows the zonal average sstClim4xCO2 cloud anomaly separately for land and for ocean. Though clouds at the highest level increase over both land and ocean, the land anomalies are much larger and in the Tropics extend over the top three  $CTP$  bins. Clouds decrease at every level from the surface to the mid-troposphere over land, whereas large increases in oceanic clouds occur in the lowest two levels. These features are likely due to the shift of convection from ocean to land following quadrupling of  $CO_2$ , as the

land heats up more rapidly than does the ocean, as shown in Wyant et al. (2012).

The vertical dipole in cloud anomalies (increases at pressures greater than 680 hPa and decreases immediately above this level) over the ocean in Figure 5 may reflect the tendency for marine boundary layer cloud tops to descend as the boundary layer shoals (Watanabe et al. (2011); Wyant et al. (2012)) and for cloud fractions to reduce due to warming and reductions in relative humidity at mid-levels (Colman and McAvaney (2011)). This feature may be apparent at a higher altitude than shown in previous studies because of our use of the ISCCP simulator (as discussed above). This interpretation is supported by latitude-height anomalies in the model-produced (i.e., non-ISCCP simulator-interpreted) cloud fields (not shown), which closely resemble the anomaly pattern shown in Figure 2a of Colman and McAvaney (2011).

The ensemble mean  $\Delta T_s$ -mediated cloud anomalies are shown in Figure 4. High clouds in all thickness categories show increases in the equatorial Pacific straddled to the north and south by negative anomalies, as convection shifts onto the equator. Negative high cloud anomalies are also evident over the tropical land masses, a notable contrast from their rapid adjustment to  $CO_2$ . High, thick cloud fraction increases substantially in the global mean, especially in the tropics, over the high latitude in the Northern Hemisphere, and over the Southern Ocean. These cloud changes lead to a strong positive LW high cloud feedback (Table 4). At mid-levels, thin and medium-thickness clouds decrease while thick clouds increase in the global mean, though their anomalies and induced feedbacks are fairly small at every location. Thin and medium-thickness low clouds decrease in the global mean, with the former primarily occurring at high latitudes and the latter occurring throughout the ocean basins equatorward of about  $60^\circ$ . Medium-thickness low clouds exhibit large reductions in coverage over the stratus regions in every basin, and espe-

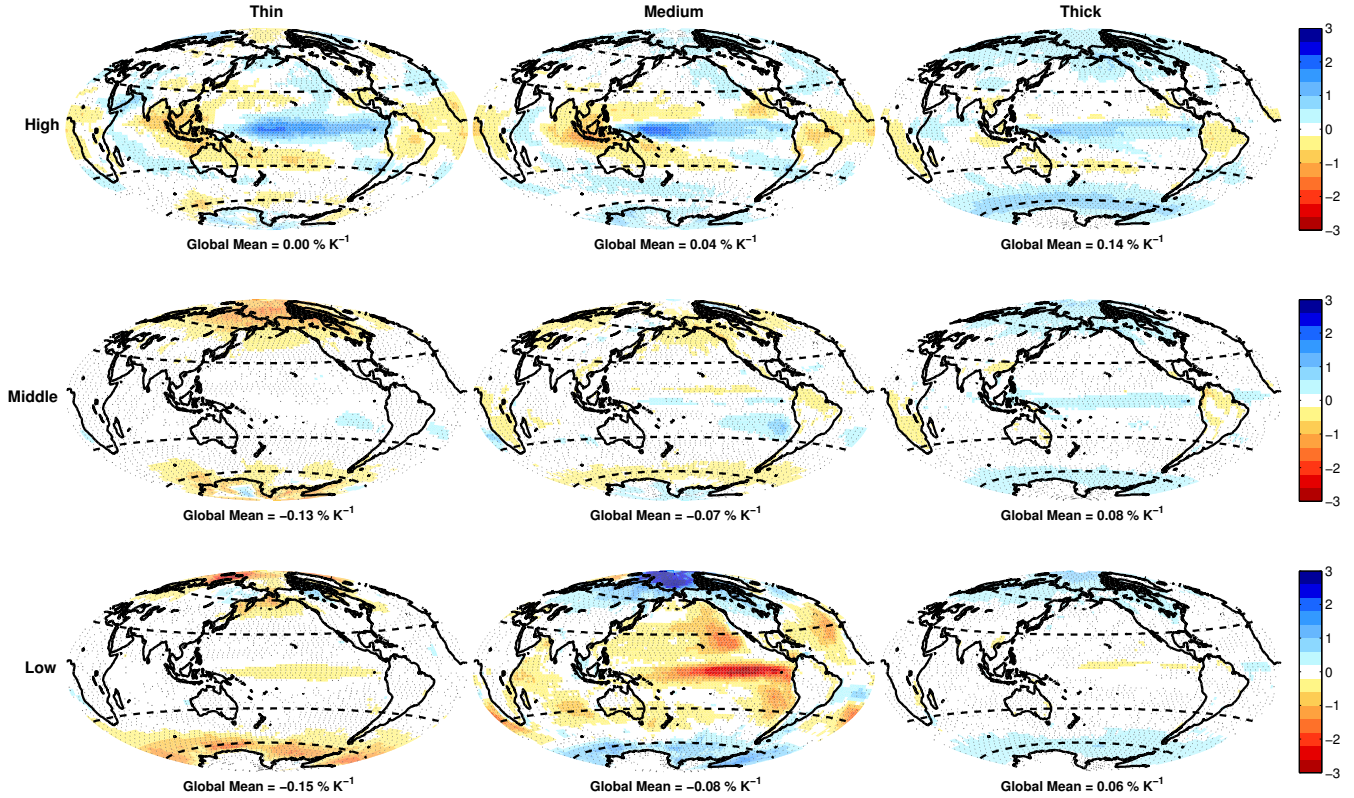


FIG. 4. Annual and ensemble mean  $\Delta T_s$ -mediated cloud anomalies partitioned into nine standard ISCCP categories. The values at each location represent the slope of the best-fit line of the local cloud fraction anomaly regressed on global mean surface temperature anomaly. Stippling indicates locations where at least 4 out of 5 models agree on the sign of the field plotted.

cially along the cold tongue in the Eastern Pacific. These changes are in striking contrast to the direct response to  $\text{CO}_2$  shown in Figure 3, and lead to a strong positive low cloud feedback.

As an attempt to synthesize the changes to cloud properties evident in Figures 3 - 5, in Figure 6 we show the changes in gross cloud properties for both the rapid responses to  $\text{CO}_2$  and the  $\Delta T_s$ -mediated responses that govern the cloud feedback. Upon  $\text{CO}_2$  quadrupling, cloud amount decreases over the Indian Ocean, tropical Atlantic Ocean and over most land areas except Africa, while generally increasing over the subtropical and midlatitude oceans. Cloud top pressure decreases significantly over land upon  $\text{CO}_2$  quadrupling, but decreases slightly over the subtropics due to an increase in low level cloud fraction rather than a downward translation of cloud tops. Indeed, high cloud altitude increases uniformly upon quadrupling (not shown). A large reduction in  $\tau$  occurs at all altitudes, especially in the Tropics, in response to quadrupled  $\text{CO}_2$ . This may be due to the significantly perturbed atmospheric energy budget following  $\text{CO}_2$  quadrupling: The reduction in

atmospheric LW cooling would necessitate a reduction in latent heat release from condensation (Bala et al. (2010)), which could plausibly lead to a reduction in cloud water and hence  $\tau$ , particularly in deep convective regions.

As the planet warms, the global mean cloud amount and  $CTP$  continue to decrease, but the patterns of these changes are in many cases of opposite sign to their rapid adjustment counterparts. Total cloud fraction decreases with increasing temperature in the subtropics and over tropical land areas and increases at higher latitudes and over the central and western Pacific. Cloud altitude increases occur over all oceanic areas except over the Arctic, and over the tropical land masses. Cloud optical depth increases substantially, especially for cold clouds at high latitudes and altitudes, as was shown in Tsushima et al. (2006) and Zelinka et al. (2012b). Toggling between Figures 3 and 4 and between the two columns in Figures 5 and 6, it is clear that in some locations the cloud adjustments act in opposition to and in other locations act in the same direction as the cloud feedbacks. These features have important consequences for feedbacks that are computed without ac-

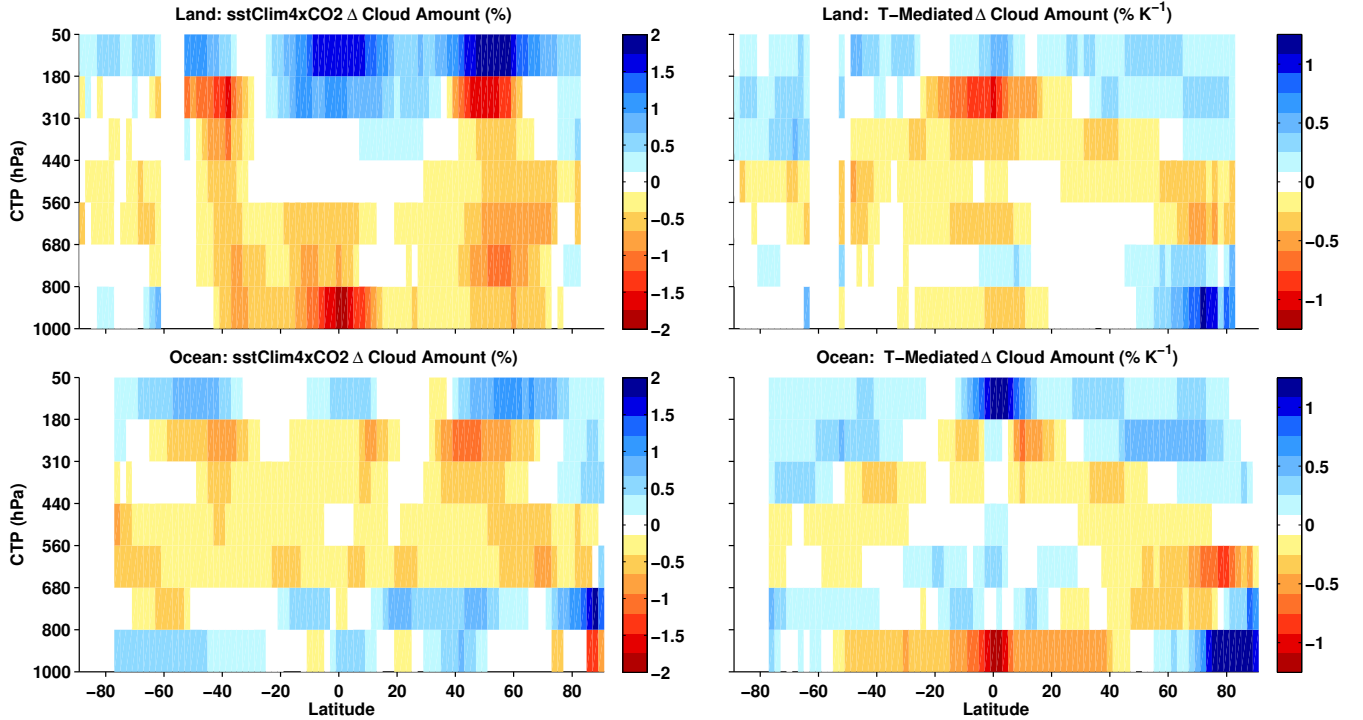


FIG. 5. Ensemble mean (left column) rapid cloud adjustments and (right column)  $\Delta T_s$ -mediated cloud anomalies over (top) land and (bottom) ocean. Only locations in which at least (left) 3 out of 4 and (right) 4 out of 5 models agree on the sign of the field are displayed. Note that the units and colorbars in each column are different.

counting for rapid cloud adjustments, as will be discussed in Section 5b.

Maps of the TOA radiation anomalies due to rapid cloud adjustments and  $\Delta T_s$ -mediated cloud anomalies are shown in Figure 7. Though the rapid cloud adjustments that occur upon quadrupling of  $\text{CO}_2$  lead to a large positive global mean SW anomaly, the component of the cloud-induced SW anomalies that evolves with surface temperature is identically zero in this ensemble of models. Thus, all of the enhanced absorbed SW radiation that would otherwise be attributed to SW cloud feedback is arising purely from abrupt cloud changes rather than as a steadily increasing SW absorption anomaly over the course of the run. This is quite similar to the results of Andrews and Forster (2008) and Andrews et al. (2012a). The opposite is the case in the LW: rapid cloud adjustments are essentially negligible, while the cloud-induced LW anomalies increase linearly with increasing global mean surface temperature. Thus, in this ensemble, nearly all of the enhanced LW heating due to clouds is indeed attributable to LW cloud feedback rather than to abrupt cloud changes, in agreement with Colman and McAvaney (2011) and Andrews et al. (2012a). It is noteworthy that the net adjustment and feedback maps are dominated by positive values at most regions, with only small portions of the midlatitude

and subtropical oceans having negative net adjustments and the high latitude oceans having negative cloud feedbacks. In sum, both rapid cloud adjustments and cloud feedbacks contribute to an enhancement in downwelling TOA net (LW+SW) radiation in the ensemble mean: Enhanced SW absorption due to cloud fraction reductions occurs immediately upon introduction of the forcing agent and remains roughly constant as the planet warms, while enhanced LW trapping due primarily to increasing cloud top altitude occurs solely as a  $\Delta T_s$ -mediated process, as expected from theory (Hartmann and Larson (2002)). It is important to bear in mind, however, that even in the ensemble mean, there are large local  $\Delta T_s$ -mediated SW cloud anomalies and instantaneous LW cloud anomalies (Figure 7), and even in the global mean, the SW cloud feedbacks are substantial within individual models (Figure 2).

Several features that were identified in the CFMIP1 slab ocean model ensemble analyzed by Zelinka et al. (2012a) continue to hold in this ensemble of CMIP5 models. First, the high and low net cloud feedbacks are robustly positive in all five models (Table 4). Second, the inter-model spread in LW and SW high cloud feedback is much larger than that due to low clouds (standard deviations of 0.4 versus  $0.2 \text{ W m}^{-2} \text{ K}^{-1}$ ), but the inter-model spread in net cloud feedback is dominated by low clouds owing to compensa-

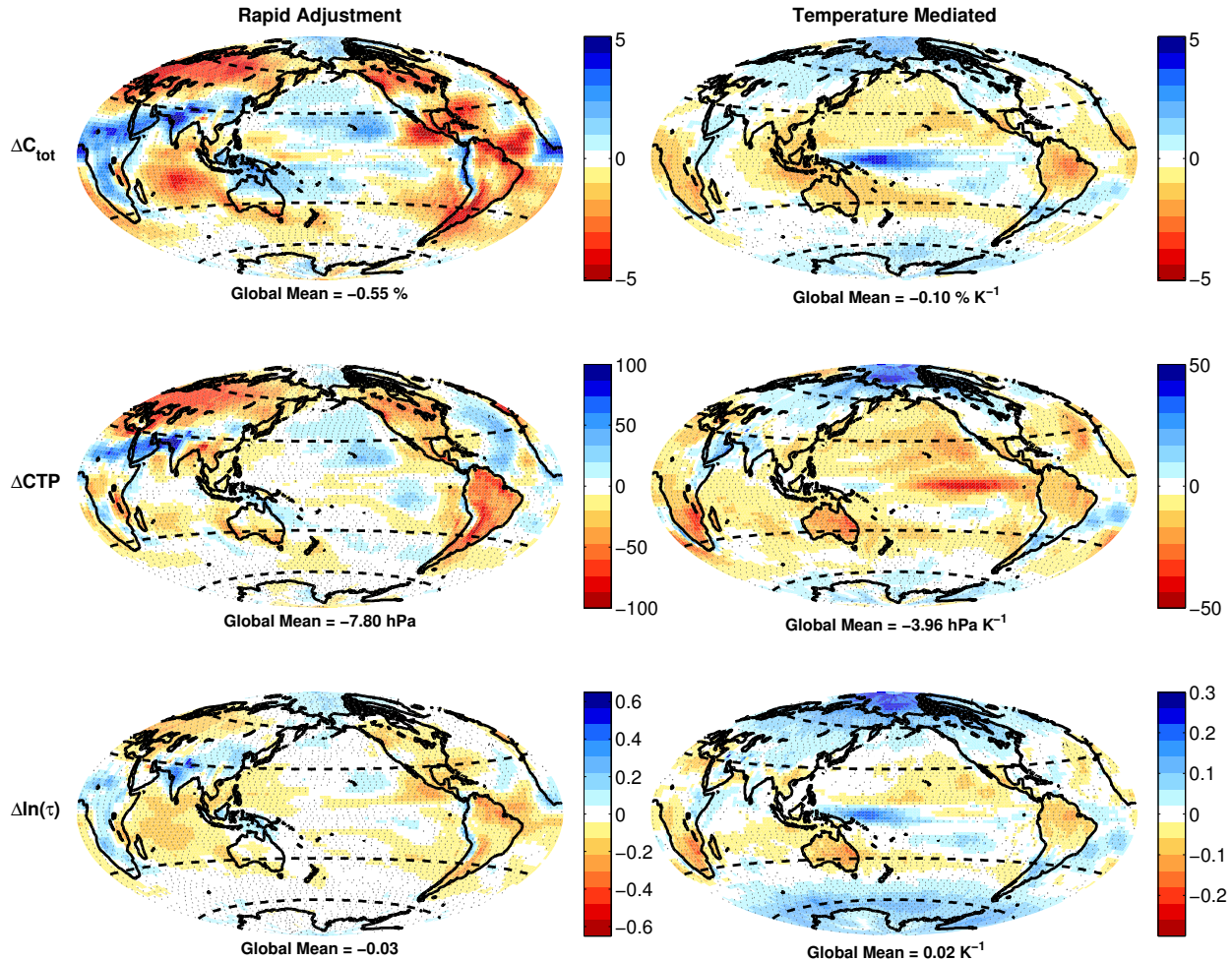


FIG. 6. Ensemble mean (left column) rapid adjustments in (top) total cloud amount, (middle) logarithm of  $\tau$ , and (bottom) CTP. (right column) Same as left column, but for  $\Delta T_s$ -mediated cloud changes. Note that the units and colorbars in each panel are different. Stippling indicates locations where at least (left) 3 out of 4 and (right) 4 out of 5 models agree on the sign of the field plotted.

tion between the LW and SW effects of high clouds (Table 4). As in CFMIP1, medium-thickness cloud reductions are the single largest contributor to the positive net cloud feedback, and contribute positively in every model. In stark contrast to the results from CFMIP1, the contribution to SW and net cloud feedback from mid-level cloud anomalies is small and negative in the ensemble mean ( $-0.03 \pm 0.12 \text{ W m}^{-2} \text{ K}^{-1}$ ). If we ignore rapid cloud adjustments and compute the mid-level cloud feedback "naively" (see Section 5b), the CMIP5 ensemble mean mid-level cloud feedback becomes  $0.19 \text{ W m}^{-2} \text{ K}^{-1}$ , very close to the value derived in the same manner for CFMIP1. This suggests (though not conclusively) that a large portion of the positive mid-level cloud feedback diagnosed in CFMIP1 was actually due to rapid mid-level cloud reductions upon doubling of  $\text{CO}_2$ .

Following the decomposition of cloud anomalies introduced in Zelinka et al. (2012b), but with modifications explained in the Appendix, we show in Table 5 the contributions of changes in cloud amount, altitude, and optical depth to the LW, SW, and net cloud feedbacks and rapid adjustments<sup>3</sup>. The global mean SW and LW radiation anomalies due to these gross cloud property changes are plotted as a function of global mean surface temperature anomaly in the right column of Figures 1 and 2.

<sup>3</sup>As noted in Zelinka et al. (2012b), aliasing can occur when such a decomposition is applied over the full ISCCP simulator histogram (e.g., large reductions solely in low clouds can cause a large positive LW cloud altitude feedback when in reality the low cloud anomalies would have little effect on OLR). It is important to bear in mind that such effects are included here, though they do not significantly affect the interpretation.

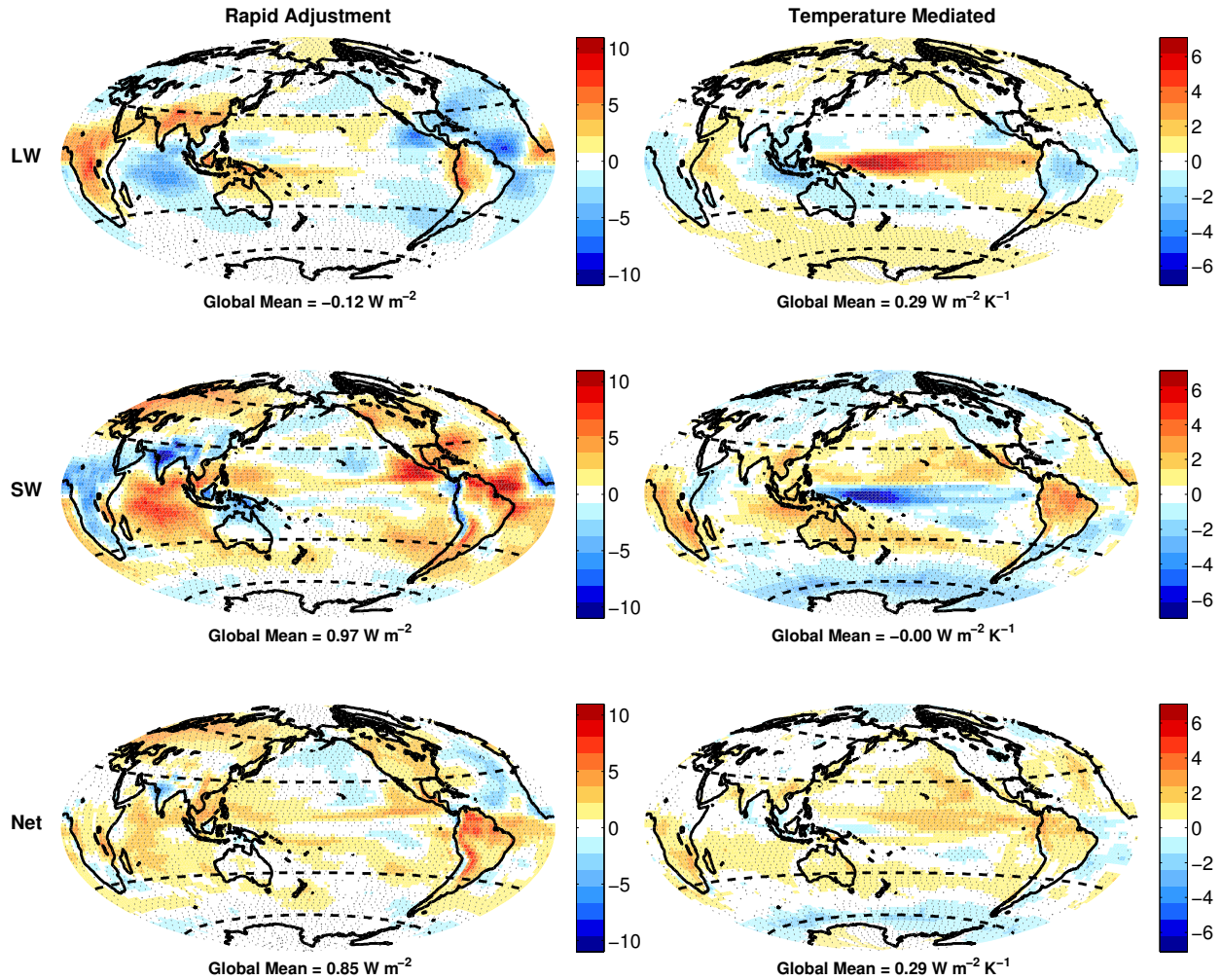


FIG. 7. Ensemble mean (top) LW, (middle) SW, and (bottom) net radiation anomalies due to (left column) rapid cloud adjustments and (right column)  $\Delta T_s$ -mediated cloud changes. Note that the units and colorbars in each column are different. Stippling indicates locations where at least (left) 3 out of 4 and (right) 4 out of 5 models agree on the sign of the field plotted.

The small negative LW cloud adjustment is caused by increases in cloud altitude nearly canceling reductions in cloud amount, with an additional small negative component coming from rapid thinning of clouds. In contrast, decreases in cloud amount and optical depth reinforce each other, leading to large positive SW cloud adjustment. The net cloud adjustment is thus quite strongly positive due to nearly equal contributions from decreases in amount,  $CTP$ , and  $\tau$ .

The LW cloud altitude feedback is robustly positive, with very little inter-model spread, and is supplemented in 4 out of 5 models by a smaller positive LW cloud optical depth feedback. The robustly positive SW cloud amount feedback is roughly twice as large as the robustly negative LW cloud amount feedback, while the negative SW

optical depth feedback is roughly four times greater than the positive LW optical depth feedback, making it the only negative contributor to the net cloud feedback. The SW and net optical depth feedback is negative in all but the *MRI-CGCM3* model, in which it is statistically indistinguishable from zero. Thus the ensemble mean positive net cloud feedback arises from positive amount and altitude feedbacks, opposed by a negative optical depth feedback.

## 5. Implications of Diagnostic and Methodological Choices

### a. Sensitivity to Diagnostics

In Figure 8 we show the cloud-induced LW anomaly, the *LWCRE* anomaly, and their difference, averaged across

TABLE 5. Global mean LW, SW, and net cloud feedbacks separated into contributions from changes in cloud amount, altitude, and optical depth following the decomposition shown in the Appendix. The uncertainty is the standard deviation across model means.

Band	CloudAdjustment ( $\text{W m}^{-2}$ )			Cloud Feedback ( $\text{W m}^{-2} \text{K}^{-1}$ )		
	Amount	Altitude	Optical Depth	Amount	Altitude	Optical Depth
LW	$-0.27 \pm 0.18$	$0.26 \pm 0.23$	$-0.07 \pm 0.05$	$-0.14 \pm 0.10$	$0.37 \pm 0.23$	$0.05 \pm 0.06$
SW	$0.59 \pm 0.38$	$-0.01 \pm 0.05$	$0.38 \pm 0.24$	$0.27 \pm 0.18$	$-0.06 \pm 0.05$	$-0.21 \pm 0.13$
Net	$0.31 \pm 0.23$	$0.25 \pm 0.18$	$0.31 \pm 0.20$	$0.13 \pm 0.09$	$0.31 \pm 0.19$	$-0.16 \pm 0.12$

the four *sstClim4xCO2* simulations. The global mean instantaneous *LWCRE* anomalies (Figure 8b) are quite strongly negative, from which one might infer a large cloud response to  $\text{CO}_2$  that reduces the forcing due to  $\text{CO}_2$ . In contrast, the global mean true LW cloud adjustment (Figure 8a) is quite small, though it locally exhibits large values of either sign. The difference map between cloud-induced OLR anomalies and *LWCRE* anomalies (Figure 8c) exhibits relatively uniform positive values that closely tracks the mean state high cloud distribution (see also Figure 1 of Wyant et al. (2012)). This difference map provides an estimate of the so-called cloud masking of the radiative perturbations arising from quadrupled  $\text{CO}_2$  concentrations and from any rapid responses of temperature and water vapor. The masking of the forcing, which is likely to be dominant, arises because the radiative forcing from  $\text{CO}_2$  is larger under clear-sky than under cloudy-sky conditions, and the magnitude of this forcing difference increases with the altitude of cloud tops. This means that immediately upon quadrupling  $\text{CO}_2$ , the *LWCRE* experiences a negative anomaly that has nothing to do with *changes* in clouds but rather simply because clouds mask the forcing. Of course, clouds also change upon introduction of  $\text{CO}_2$ , and this is what is captured by the cloud radiative kernel values. We derive a LW masking of roughly  $1.3 \text{ W m}^{-2}$ , quite close to estimates given in Soden et al. (2008), Colman and McAvaney (2011), and Andrews et al. (2012a). For the *HadGEM2 - ES* model, we derive a global mean LW masking ( $1.12 \text{ W m}^{-2}$ ) identically equal to that derived independently with offline radiation calculations shown in Figure 1 of Wyant et al. (2012).

In contrast, the instantaneous *SWCRE* anomaly is slightly more positive than the cloud-induced SW flux anomaly (not shown). Thus the SW cloud forcing mask is of opposing sign and is much smaller than its LW counterpart. This is because the cloud masking effect works in the opposite sense in the SW: the presence of clouds – especially low clouds – increases the average path length over which solar photons travel, slightly increasing their likelihood of being absorbed by the increased number of  $\text{CO}_2$  molecules.

The use of *CRE* as a diagnostic also has implications for computing cloud feedback, for essentially the same reasons.

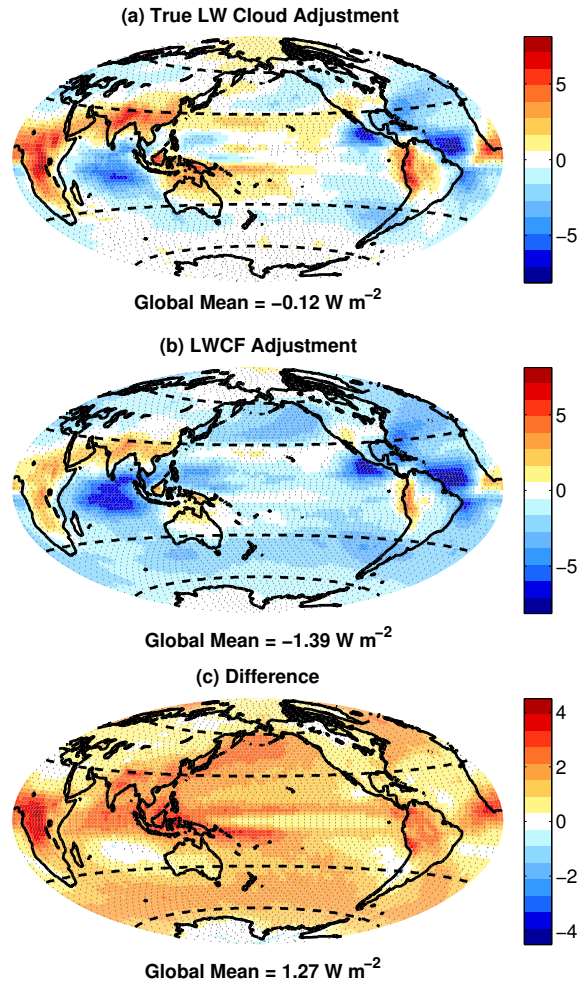


FIG. 8. Ensemble mean (a) true and (b) *CRE*-derived LW rapid cloud adjustments diagnosed from the *sstClim4xCO2* simulations, along with (c) their difference. Note that the colorbars in (a) and (b) range from  $-8$  to  $8 \text{ W m}^{-2}$  whereas that in (c) ranges from  $-4.5$  to  $4.5 \text{ W m}^{-2}$ . Stippling indicates locations where at least 3 out of 4 models agree on the sign of the field plotted.

Because  $CRE$  anomalies can be caused by changes in non-cloud fields, the change in  $CRE$  with temperature is in general not the same as the cloud feedback, as discussed in Soden et al. (2004) and Soden et al. (2008). In Figure 9a and b we show the net cloud feedback computed with the cloud radiative kernels and with  $\Delta CRE$  cloud feedback. Note that both of these are derived in the same manner by taking the slope of the regression line on the Gregory plot at each location. The true net cloud feedback (Figure 9a) is roughly  $0.3 \text{ W m}^{-2}\text{K}^{-1}$  greater than that derived with net  $\Delta CRE$  (Figure 9b), and is positive rather than negative. The difference map (Figure 9c) gives an estimate of the cloud masking of the non-cloud feedbacks. Large positive values over the high and low latitudes originate from clouds masking the surface albedo and water vapor feedbacks, respectively. Figure 10 of Soden et al. (2008) exhibits a very similar pattern of cloud masking in the SRES A1b scenario, but the global mean value they derive ( $0.66 \text{ W m}^{-2}\text{K}^{-1}$ ) is roughly twice as large as that derived here. Thus the cloud feedback computed with  $CRE$  as a diagnostic is biased toward more negative values. Only 1 out of 5 models in this study (*MIROC5*) has a negative net cloud feedback, whereas 3 have an implied negative feedback when computed with  $CRE$ .

#### b. Sensitivity to Methodology

Before it was recognized that clouds may undergo a rapid response due directly to the increased  $\text{CO}_2$  forcing, all cloud changes that existed at the end of a perturbed  $\text{CO}_2$  simulation were assumed to have occurred in response to increasing surface temperature, and therefore were incorporated into the feedback. One would simply take the average cloud-induced radiation anomalies at the end of the run (once it is near equilibrium) and divide by the corresponding change in global mean surface temperature to compute the feedback. We will refer to this as a "naive" calculation of the feedback, though this is in no way meant to be pejorative, as it was not known until recently that fast responses occurred, and no other option is available if model output is not archived through the duration of an abrupt forcing experiment. In Figure 9d, we show this naive calculation of the cloud feedback. Note that this feedback is computed using the cloud-induced change in radiative fluxes from the kernels rather than net  $\Delta CRE$ , so it does not include cloud masking effects.

The true net cloud feedback is only about half as large as the naively-computed net cloud feedback for this ensemble. This difference is entirely attributable to the rapid responses of clouds to quadrupled  $\text{CO}_2$  that is aliased into the naive net cloud feedback, but not included in the true cloud feedback. Compared with their naively-computed counterparts, the true LW altitude feedback is  $0.08 \text{ W m}^{-2}\text{K}^{-1}$  less positive and the true LW amount feedback is  $0.07 \text{ W m}^{-2}\text{K}^{-1}$  less negative (not shown) because of

the decrease in  $CTP$  and cloud amount that occurs immediately upon  $\text{CO}_2$  quadrupling (Figure 6). These offsetting global mean LW cloud amount and altitude adjustments mean that most of the difference between the naive and true cloud feedback arises from the SW component. Remarkably, whereas the ensemble mean naive SW cloud feedback is  $0.30 \text{ W m}^{-2}\text{K}^{-1}$ , the true SW cloud feedback is  $0.00 \text{ W m}^{-2}\text{K}^{-1}$  (not shown). The true SW amount feedback is  $0.13 \text{ W m}^{-2}\text{K}^{-1}$  less positive and the true SW optical depth feedback is  $0.18 \text{ W m}^{-2}\text{K}^{-1}$  more negative than their naively-computed counterparts owing to the rapid  $\text{CO}_2$ -induced reduction in total cloud amount and optical depth. Notably, the true SW optical depth feedback is much less positive at low latitudes and much more negative at high latitudes than its naive counterpart. As found in Zelinka et al. (2012b), the large negative feedback over the Southern Ocean comes from the shift towards thicker clouds and the increase in total cloud amount, but the former is roughly three times stronger in the zonal mean at  $60^\circ\text{S}$ . Properly accounting for the rapid cloud adjustments makes this high latitude brightening of clouds even more dramatic, and further increases the importance of cloud brightening over cloud increases in causing the high latitude negative feedback.

## 6. Conclusions

In this paper we have used output from the ISCCP simulator to illuminate the direct responses of clouds to  $\text{CO}_2$  as well as the  $\Delta T_s$ -mediated changes in clouds that progress as the planet warms across an ensemble of five CMIP5 GCMs. In addition, we have used cloud radiative kernels to quantify the radiative impact of these cloud anomalies, thereby diagnosing the true cloud feedback and rapid adjustments, with no influence from cloud masking effects that can be difficult to account for in other methods.

A spatially uniform decrease in mid-level clouds and shift from thicker to thinner cloud types occurs upon quadrupling of  $\text{CO}_2$ , while marine stratocumulus clouds and high clouds over land exhibit dramatic increases. Though these cloud anomalies have only a small negative (cooling) influence on the global mean LW budget of the planet in every model, they strongly increase the amount of SW radiation absorbed by the planet in every model, consistent with many previous studies (Andrews and Forster (2008); Colman and McAvaney (2011); Watanabe et al. (2011); Andrews et al. (2012a)). As the planet warms due to quadrupled  $\text{CO}_2$  levels, high cloud altitude continues to increase, leading to a large positive LW cloud feedback, consistent with Zelinka and Hartmann (2010) and Zelinka et al. (2012b). Unlike the direct response of clouds to  $\text{CO}_2$ , low clouds equatorward of  $60^\circ$  decrease substantially over every ocean basin as the planet warms, and cold clouds at high latitudes and altitudes become thicker, leading to

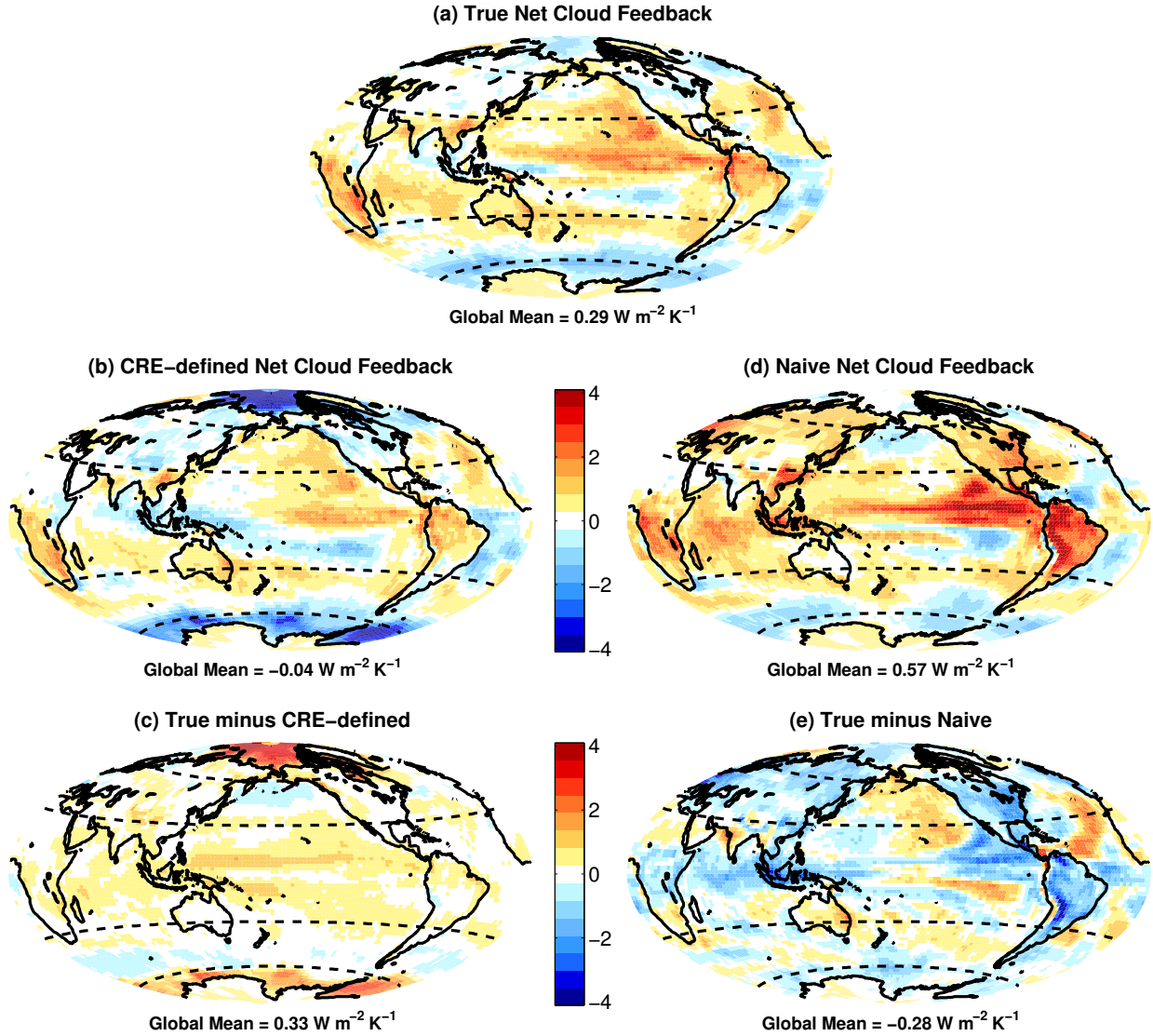


FIG. 9. Ensemble mean (a) true, (b) *CRE*-defined, and (d) naively-defined net cloud feedback diagnosed from the *abrup4xCO<sub>2</sub>* simulations. The difference between the true and *CRE*-defined feedback is shown in (c) and between the true and naively-defined feedback in (e).

positive SW cloud amount and negative SW cloud optical depth feedbacks, as also found in CFMIP1 models (Zelinka et al. (2012b)). In the ensemble mean, all of the cloud-enhanced SW heating that is present in the nearly equilibrated  $4x\text{CO}_2$  state arose from cloud reductions immediately upon introduction of the forcing agent, with little  $\Delta T_s$ -mediated response. In contrast, nearly all of the cloud-enhanced LW heating present in the nearly equilibrated  $4x\text{CO}_2$  state arose from  $\Delta T_s$ -mediated cloud top altitude increases, with little direct response to the forcing agent.

We have also highlighted the implications of diagnostic

and methodological choices on the derived cloud feedbacks and adjustments. First, we showed that *CRE*-derived LW cloud adjustments are strongly negatively biased, owing to the  $1.3 \text{ W m}^{-2}$  masking of the  $4x\text{CO}_2$  radiative forcing by clouds rather than any true cloud adjustment to  $\text{CO}_2$ . Similarly, the net cloud feedback is negatively based due to roughly  $0.3 \text{ W m}^{-2} \text{ K}^{-1}$  cloud masking of positive non-cloud feedbacks. Second, we showed that calculating cloud feedbacks by simply taking the cloud-related radiation anomalies at the end of a perturbed run and dividing by the global mean surface temperature change between equilibrium states, as is commonly done, will give the in-

correct value of the cloud feedback. This is because of the large adjustments that occur immediately upon CO<sub>2</sub> quadrupling that are better interpreted as an adjustment to the forcing than as a feedback. This primarily affects the SW cloud feedbacks, for which the (positive) amount feedback is reduced in magnitude from its naive value and the (negative) optical depth feedback is increased in magnitude from its naive value. In this ensemble, failing to account for the true time-dependent cloud-induced anomalies leads to a 100% overestimate of the net cloud feedback.

Our primary purpose in this paper was to detail the cloud anomalies responsible for rapid adjustments and feedbacks across an ensemble of currently available CMIP5 models and to quantify the effect of different methodological and diagnostic choices on the derived feedbacks and rapid adjustments. We have not attempted to explain every feature that is present in the results, and hope that this paper will motivate further study of these cloud processes. Specifically, this study has raised numerous questions, like

- Why does cloud optical depth decrease immediately following CO<sub>2</sub> quadrupling?
- According to Hartmann and Larson (2002), high clouds shift upwards in a warming climate due to the upward shift of the water vapor radiative cooling profile. Can the rapid increase in high cloud altitude be explained in the same way, but with CO<sub>2</sub> playing the role of water vapor?
- The global mean LW cloud adjustment is systematically near zero due to a remarkable cancellation of nonzero amount, altitude, and optical depth changes. Are there reasons to expect this to be negligible?
- What causes the large deviations from linearity evident in the early stages of the quadrupled simulations in some models but not in others?

As a follow-up to the final question, we note that although global mean cloud-induced radiation anomalies behave remarkably linearly for the majority of a abrupt forcing simulation, the forcing-feedback paradigm cannot fully capture the rich structure evident in the time-evolving radiative anomalies. Moreover, separation between rapid (CO<sub>2</sub> adjustment) and slow ( $\Delta T_s$ -mediated) timescales is not clear and likely varies from model to model. Thus we echo the sentiment expressed in Andrews et al. (2012b) that consideration of the time-evolving radiative anomalies is crucial for properly understanding the role of clouds in altering the radiation budget of the perturbed climate.

*Acknowledgments.*

We acknowledge the World Climate Research Programme’s Working Group on Coupled Modelling, which is responsible for CMIP, and we thank the climate modeling groups

(listed in Table 1 of this paper) for producing and making available their model output. For CMIP the U.S. Department of Energy’s Program for Climate Model Diagnosis and Intercomparison provides coordinating support and led development of software infrastructure in partnership with the Global Organization for Earth System Science Portals. The work of MDZ, SAK, and KET was supported by the Regional and Global Climate Modeling Program of the Office of Science at the U. S. Department of Energy and was performed under the auspices of the U.S. Department of Energy by Lawrence Livermore National Laboratory under Contract DE-AC52-07NA27344. TA, MJW and JMG were supported by the Joint DECC/Defra Met Office Hadley Centre Climate Programme (GA01101). MJW is also supported by funding from the European Union, Seventh Framework Programme (FP7/2007-2013) under grant agreement No. 244067 via the EU Cloud Intercomparison and Process Study Evaluation project (EUCLIPSE).

APPENDIX

**A Modified Decomposition of the Cloud Feedback**

Zelinka et al. (2012b) proposed a decomposition of the anomalous cloud fraction histogram that allowed for partitioning the cloud feedbacks into contributions from change in the total amount of clouds keeping the altitude and optical depth distribution fixed, the change in altitude keeping the total amount and optical depth distribution fixed, and the change in optical depth, keeping the total amount and altitude distribution fixed. The sum of these three components would ideally sum to the total cloud feedback, but in most cases there is a residual that arises from the fact that most cloud changes do not fall solely into one component and are therefore included in several. Here we describe the modifications we have made to the cloud feedback decomposition that reduce the size of this residual, while remaining true to the original philosophy of the decomposition.

We first express the anomalous cloud fraction ( $\Delta C_{p\tau}$ ) as

$$\Delta C_{p\tau} = \left(\frac{C_{p\tau}}{C_{tot}}\right)\Delta C_{tot} + \Delta C_{p\tau}^*, \quad (A1)$$

where

$$C_{tot} = \sum_{p=1}^P \sum_{\tau=1}^T C_{p\tau}, \quad (A2)$$

and we express the kernel as

$$K_{p\tau} = K_0 + K'_{p\tau}, \quad (A3)$$

where

$$K_0 = \sum_{p=1}^P \sum_{\tau=1}^T \left(\frac{C_{p\tau}}{C_{tot}}\right) K_{p\tau}. \quad (A4)$$

The first term on the RHS of (A1) is the hypothetical change in cloud fraction assuming the change in total cloud

fraction is distributed throughout the histogram such that the relative proportions of cloud fractions in each  $CTP$ - $\tau$  bin remains constant, and is identical to that derived in Zelinka et al. (2012b).

The cloud-induced radiation anomaly is given by

$$\Delta R_c \equiv \sum_{p=1}^P \sum_{\tau=1}^T K_{p\tau} \Delta C_{p\tau} = K_0 \Delta C_{tot} + \sum_{p=1}^P \sum_{\tau=1}^T K'_{p\tau} \Delta C_{p\tau}^* \quad (\text{A5})$$

The first term on the RHS (when divided by  $\Delta T_s$ ) is the cloud amount feedback, and is identical to that derived in Zelinka et al. (2012b). The second term on the RHS (when divided by  $\Delta T_s$ ) contains the sum of altitude, optical depth, and residual feedbacks.

We can further resolve  $K'$  into components:

$$K'_{p\tau} = K'_p + K'_\tau + K'_R, \quad (\text{A6})$$

where

$$K'_p = \sum_{\tau=1}^T (K'_{p\tau} \sum_{p=1}^P \frac{C_{p\tau}}{C_{tot}}), \quad (\text{A7})$$

$$K'_\tau = \sum_{p=1}^P (K'_{p\tau} \sum_{\tau=1}^T \frac{C_{p\tau}}{C_{tot}}), \quad (\text{A8})$$

and

$$K'_R = K'_{p\tau} - K'_p - K'_\tau. \quad (\text{A9})$$

The cloud-induced radiation anomalies are then expressed as

$$\Delta R_c = K_0 \Delta C_{tot} + \sum_{p=1}^P (K'_p \sum_{\tau=1}^T \Delta C_{p\tau}^*) + \sum_{\tau=1}^T (K'_\tau \sum_{p=1}^P \Delta C_{p\tau}^*) + \sum_{p=1}^P \sum_{\tau=1}^T K'_R \Delta C_{p\tau}^* \quad (\text{A10})$$

The terms on the RHS (when divided by  $\Delta T_s$ ) are the cloud amount, altitude, optical depth, and residual feedbacks, respectively.

## REFERENCES

- Andrews, T. and P. M. Forster, 2008: CO2 forcing induces semi-direct effects with consequences for climate feedback interpretations. *Geophys. Res. Lett.*, **35**, L04802, doi:10.1029/2007GL032273.
- Andrews, T., J. Gregory, P. Forster, and M. Webb, 2012a: Cloud adjustment and its role in CO2; radiative forcing and climate sensitivity: A review. *Surveys in Geophysics*, **33**, 619–635, doi:10.1007/s10712-011-9152-0.
- Andrews, T., J. M. Gregory, M. J. Webb, and K. E. Taylor, 2012b: Forcing, feedbacks and climate sensitivity in cmip5 coupled atmosphere-ocean climate models. *Geophys. Res. Lett.*, **39**, L09712, doi:10.1029/2012GL051607.
- Bala, G., K. Caldeira, and R. Nemani, 2010: Fast versus slow response in climate change: implications for the global hydrological cycle. *Climate Dynamics*, **35**, 423–434, doi:10.1007/s00382-009-0583-y.
- Cess, R. D., 1974: Radiative transfer due to atmospheric water vapor: Global considerations of Earth's energy balance. *Journal of Quantitative Spectroscopy and Radiative Transfer*, **14** (9), 861–871.
- Cess, R. D., 1975: Global climate change - investigation of atmospheric feedback mechanisms. *Tellus*, **27** (3), 193–198.
- Charney, J. G. e. a., 1979: Carbon dioxide and climate: A scientific assessment. National Academy of Science, 22 pp.
- Collins, W. J., et al., 2011: Development and evaluation of an Earth-system model - HadGEM2. *Geosci. Model Dev. Discuss.*, **4**, 997–1062.
- Colman, R., J. Fraser, and L. Rotstayn, 2001: Climate feedbacks in a general circulation model incorporating prognostic clouds. *Climate Dyn.*, **18**, 103–122.
- Colman, R. and B. McAvaney, 2011: On tropospheric adjustment to forcing and climate feedbacks. *Climate Dyn.*, 1–10.
- Dufresne, J.-L. and S. Bony, 2008: An assessment of the primary sources of spread of global warming estimates from coupled atmosphere–ocean models. *Journal of Climate*, **21** (19), 5135–5144, doi:10.1175/2008JCLI2239.1.
- Fu, Q. and K. N. Liou, 1993: Parameterization of the solar radiative properties of cirrus clouds. *J. Atmos. Sci.*, **50**, 2008–2025.
- Garay, M. J., S. P. de Szoeke, and C. M. Moroney, 2008: Comparison of marine stratocumulus cloud top heights in the southeastern Pacific retrieved from satellites with coincident ship-based observations. *J. Geophys. Res.*, **113**, D18204, doi:10.1029/2008JD009975.
- Good, P., J. Gregory, and J. A. Lowe, 2011: A step?response simple climate model to reconstruct and interpret AOGCM projections. *Geophys. Res. Lett.*, **38**, L01703, doi:10.1029/2010GL045208.
- Good, P., J. Gregory, J. A. Lowe, and T. Andrews, 2012: Abrupt CO2 experiments as tools for predicting and understanding CMIP5 representative concentration pathway projections. *Climate Dyn.*, doi:10.1007/s00382-012-1410-4.
- Gregory, J. and M. Webb, 2008: Tropospheric adjustment induces a cloud component in CO2 forcing. *J. Climate*, **21** (1), 58–71.

- Gregory, J. M., et al., 2004: A new method for diagnosing radiative forcing and climate sensitivity. *Geophysical Research Letters*, **31** (3), L03205, doi:10.1029/2003GL018747.
- Hartmann, D. L. and K. Larson, 2002: An important constraint on tropical cloud-climate feedback. *Geophys. Res. Lett.*, **29** (20), doi:10.1029/2002GL015835.
- Klein, S. A. and D. L. Hartmann, 1993: The seasonal cycle of low stratiform clouds. *J. Climate*, **6**, 1587–1606.
- Klein, S. A. and C. Jakob, 1999: Validation and sensitivities of frontal clouds simulated by the ECMWF model. *Mon. Weath. Rev.*, **127**, 2514–2531.
- Meehl, G. A. et al., 2007: Global climate projections. *Climate Change 2007: The Physical Science Basis*, S. S. et al., Ed., Cambridge University Press, 747–846.
- Raddatz, T. J. et al., 2007: Will the tropical land biosphere dominate the climate-carbon cycle feedback during the twenty first century? *Climate Dyn.*, **29**, 565–574, doi:10.1007/s00382-007-0247-8.
- Rossow, W. B. and R. A. Schiffer, 1999: Advances in understanding clouds from ISCCP. *Bull. Amer. Meteor. Soc.*, **80** (11), 2261–2287.
- Schneider, S. H., 1972: Cloudiness as a global climatic feedback mechanism: The effects on radiation balance and surface-temperature of variations in cloudiness. *J. Atmos. Sci.*, **29** (8), 1413–1422.
- Schneider, S. H. and R. E. Dickinson, 1974: Climate modeling. *Reviews of Geophysics*, **12** (3), 447–493.
- Senior, C. and J. Mitchell, 1993: Carbon dioxide and climate. The impact of cloud parameterization. *J. Climate*, **6**, 393–418.
- Shell, K. M., J. T. Kiehl, and C. A. Shields, 2008: Using the radiative kernel technique to calculate climate feedbacks in NCAR’s Community Atmospheric Model. *J. Climate*, **21** (10), 2269–2282.
- Soden, B. J., A. J. Broccoli, and R. S. Hemler, 2004: On the use of cloud forcing to estimate cloud feedback. *J. Climate*, **17**, 3661–3665.
- Soden, B. J. and I. M. Held, 2006: An assessment of climate feedbacks in coupled ocean-atmosphere models. *J. Climate*, **19**, 3354–3360.
- Soden, B. J., I. M. Held, R. Colman, K. M. Shell, J. T. Kiehl, and C. A. Shields, 2008: Quantifying climate feedbacks using radiative kernels. *J. Climate*, **21**, 3504–3520.
- Taylor, K. E., R. J. Stouffer, and G. A. Meehl, 2012: An overview of cmip5 and the experiment design. *BAMS*, **93** (4), 485–498, doi:10.1175/BAMS-D-11-00094.1.
- Tsushima, Y., et al., 2006: Importance of the mixed-phase cloud distribution in the control climate for assessing the response of clouds to carbon dioxide increase: A multi-model study. *Climate Dyn.*, **27**, 113–126.
- Watanabe, M., H. Shiogama, M. Yoshimori, T. Ogura, T. Yokohata, H. Okamoto, S. Emori, and M. Kimoto, 2011: Fast and slow timescales in the tropical low-cloud response to increasing CO<sub>2</sub> in two climate models. *Climate Dynamics*, 1–15, doi:10.1007/s00382-011-1178-y.
- Watanabe, M. et al., 2010: Improved climate simulation by MIROC5: Mean states, variability, and climate sensitivity. *J. Climate*, **23**, 6312–6335.
- Webb, M., F. Lambert, and J. Gregory, 2012: Origins of differences in climate sensitivity, forcing and feedback in climate models. *Climate Dynamics*, 1–31, URL <http://dx.doi.org/10.1007/s00382-012-1336-x>, 10.1007/s00382-012-1336-x.
- Webb, M., C. Senior, S. Bony, and J. J. Morcrette, 2001: Combining ERBE and ISCCP data to assess clouds in the Hadley Centre, ECMWF and LMD atmospheric climate models. *Climate Dyn.*, **17**, 905–922.
- Wetherald, R. and S. Manabe, 1988: Cloud feedback processes in a general circulation model. *J. Atmos. Sci.*, **45**, 1397–1415.
- Wood, R. and C. S. Bretherton, 2006: On the relationship between stratiform low cloud cover and lower-tropospheric stability. *J. Climate*, **19** (24), 6425–6432.
- Wyant, M. C., C. S. Bretherton, P. N. Blossey, and M. Khairoutdinov, 2012: Fast cloud adjustment to increasing CO<sub>2</sub> in a superparameterized climate model. *J. Adv. Model. Earth Syst.*, **4**.
- Yukimoto, S. et al., 2011: Meteorological research institute – earth system model version 1 (MRI-ESM1): Model Description. *Technical Report No. 64*, Meteorological Research Institute, Tsukuba city, Ibaraki 305-0052, Japan, 96 pp.
- Zelinka, M. D. and D. L. Hartmann, 2010: Why is longwave cloud feedback positive? *J. Geophys. Res.*, **115**, D16117, doi:10.1029/2010JD013817.
- Zelinka, M. D., S. A. Klein, and D. L. Hartmann, 2012a: Computing and partitioning cloud feedbacks using cloud property histograms. Part I: Cloud radiative kernels. *J. Climate*, **25**, doi:10.1175/JCLI-D-11-00248.1.

Zelinka, M. D., S. A. Klein, and D. L. Hartmann, 2012b: Computing and partitioning cloud feedbacks using cloud property histograms. Part II: Attribution to changes in cloud amount, altitude, and optical depth. *J. Climate*, **25**, 3736–3754, doi:10.1175/JCLI-D-11-00249.1.